ACS OMEGA

Open Access

http://pubs.acs.org/journal/acsodf

Article

Zinc Complexes of Cationic Ammonium Phenyl and Methylpyridinium Porphyrins Display Synergistic Anti-HIV-1 and Broad-Spectrum Antibacterial Activity

Debdulal Sharma, Madhu Rai, Nandita Das, Ravi Kumar Kapavarapu, Piyush Pandey,* Ritu Gaur,* and Devashish Sengupta*

Cite This: *ACS Omega* 2025, 10, 22482−22507

Read Online

ACCESS | Metrics & More | Article Recommendations | Supporting Information

ABSTRACT: This study presents a pioneering series of cationic porphyrins with promising synergistic antimicrobial and anti-HIV properties, particularly effective against drug-resistant strains. The synthesized porphyrins, including **P_3AmM**, **PAm_3M**, and **c-P_2Am_2M**, as well as their zinc(II) complexes (**P_3AmZM**, **PAm_3ZM**, and **c-P_2Am_2ZM**), were developed through strategic methylation of primary amino groups in precursor porphyrins, addressing steric challenges associated with repetitive amine alkylation. Under photodynamic therapy (PDT) conditions, these compounds exhibited notable suppression of HIV-1 entry and infection, in addition to demonstrating potent antibacterial activity against drug-resistant *Escherichia coli* and *Staphylococcus aureus*. Bacterial growth kinetics indicated reduced proliferation and biofilm formation over a five-day period, underscoring their efficacy as antibacterial agents. Compounds **P_3AmZM**, **PAm_3ZM**, **c-P_2Am_2M**, **c-P_2Am_2ZM**, and **PAm_3M** displayed enhanced antibacterial potency, with *S. aureus* showing greater susceptibility. Disc diffusion assays further confirmed the superior efficacy of **c-P_2Am_2M** and **c-P_2Am_2ZM**, particularly against *S. aureus*. Computational molecular docking simulations highlighted the robust binding affinity and interaction profiles of **c-P_2Am_2M** and **c-P2Am_2ZM** with key HIV targets. These findings position these novel cationic porphyrins as potential dual-action therapeutics, combining synergistic anti-HIV efficacy with potent antibacterial activity under PDT conditions.

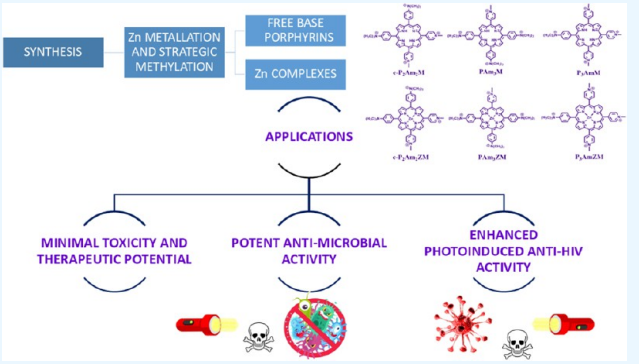

1. INTRODUCTION

Developing effective therapeutic strategies against viral and bacterial infections remains a critical global challenge, particularly due to the escalating issue of drug resistance.[1−14] Synthetic photosensitizers (PSs) have emerged as innovative agents, leveraging photodynamic therapy (PDT) to selectively eradicate cancer cells, bacteria, and viruses through light-activated production of cytotoxic species. This approach addresses limitations in traditional antiviral and antibacterial treatments, proving particularly effective against drug-resistant strains of *Staphylococcus aureus*, *Escherichia coli*, and viruses such as HIV, hepatitis, and influenza.[15−18] Notably, porphyrins, as PSs, exhibit antibacterial properties, disrupting Gram-negative bacterial lipid membranes through their hydrophobic components. Metalloporphyrins have also shown broad-spectrum efficacy against both Gram-positive and Gram-negative bacteria.[16−18]

Cationic porphyrins (CPs), particularly those containing nitronium derivatives, have been extensively studied for applications in cancer PDT (cPDT), antimicrobial PDT (aPDT), and antiviral therapies.[1−12] Alternative cationic groups, such as phosphonium and sulfonium, have shown specific anticancer and anti-HIV activities, respectively.[11,13,14] Structural modifications, such as incorporating longer alkyl chains or trifluoromethyl groups, further optimize cellular uptake and lipophilicity.[19] Porphyrins with balanced hydrophilic and lipophilic properties, achieved by appending cationic and neutral groups at *meso*-positions, have shown enhanced activity. For example, tetra-cationic porphyrins, featuring *meso*-trimethylammonium substitutions, display significant efficacy against *Candida albicans* and *E. coli*, attributed to their superior cellular uptake via self-promoted pathways. This distinguishes tetra-cationic CPs from their mono-, di-, and tri-cationic counterparts.[12,13,20−23] The observed antibacterial effect aligns with the first report of bactericidal activity of quaternary ammonium cations (QACs) by Jacobs and the subsequent

Received: October 19, 2024
Revised: April 4, 2025
Accepted: April 29, 2025
Published: May 28, 2025

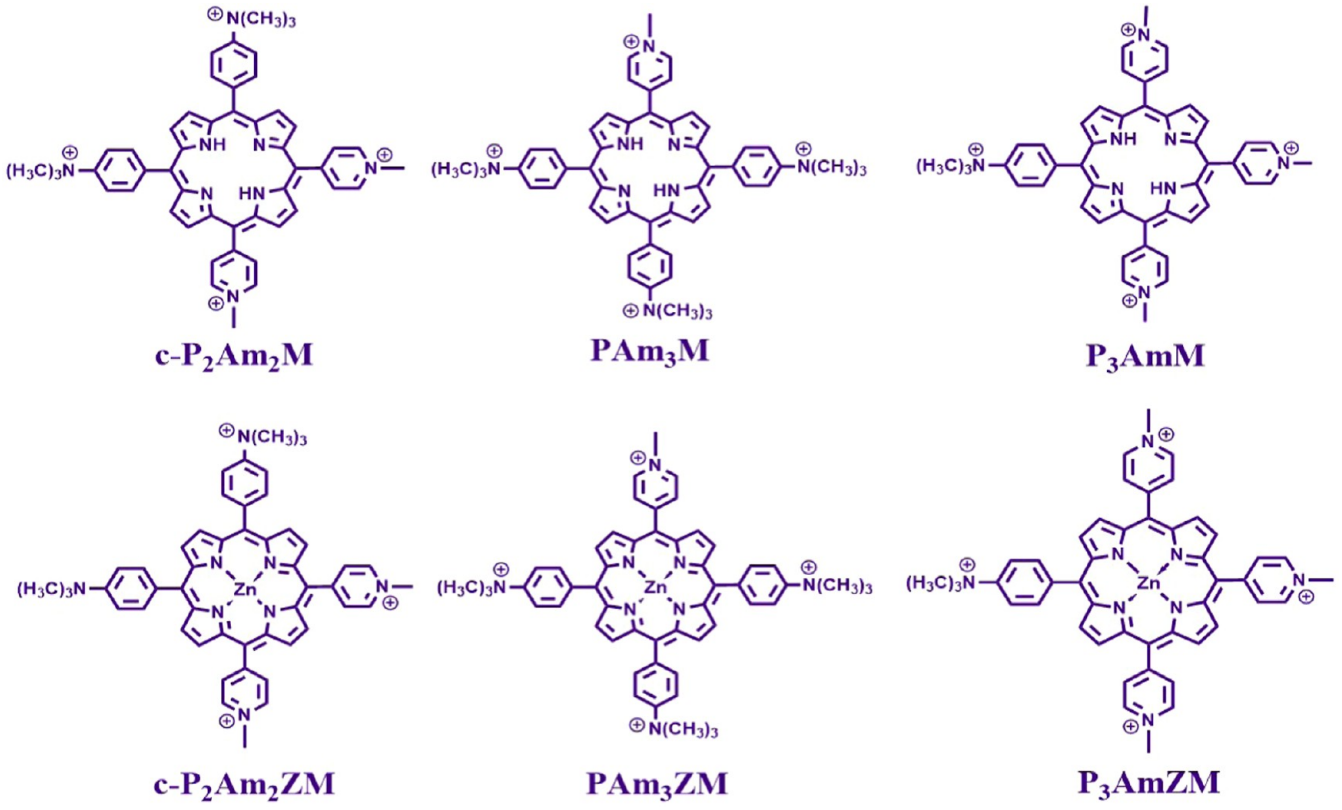

Figure 1. Synthesized water-soluble ammonium phenyl porphyrins **P_3AmM**, **c-P_2Am_2M**, **PAm_3M**, and their corresponding Zn (II) metal complexes **P_3AmZM**, **c-P_2Am_2ZM**, **PAm_3ZM**.

development of a diverse range of compounds having antibacterial and antifungal properties.[24]

Metalloporphyrins represent a promising class of PSs due to their dual light-dependent and independent antimicrobial properties.[25] Protoporphyrin IX-derived metalloporphyrins, which exploit bacterial heme uptake systems, show potential as antibiotic alternatives.[26] However, strains lacking these pathways demonstrate resistance.[26] Manganese porphyrins, functioning as superoxide dismutase (SOD) mimics, are particularly noteworthy for their minimal toxicity to eukaryotic cells, with several therapies currently in Phase II clinical trials. These manganese-based porphyrins hold promise in reducing oxidative stress and providing antimicrobial benefits without harming human cells.[27] Similarly, Zn-porphyrin nanodisks, under visible light irradiation, demonstrate remarkable antibacterial activity against *E. coli*, attributed to efficient singlet oxygen generation. Symmetric cationic porphyrins, such as TMAPP, have been successfully applied in cPDT, while mixed cationic groups like *meso*-(4-trimethylammonium phenyl) and *meso*-(4-methylpyridinium) present opportunities for enhanced photobiological applications, warranting further investigation.[20,21,28−32] The concoction of positive charges from different chemical environments can be expected to develop into interesting photobiological outcomes. Structural modifications position these molecules as promising candidates for developing innovative agents against diverse pathogenic microbes.[33] Individuals with HIV, due to compromised immunity, face higher risks of infections from *S. aureus* and *E. coli*. Research has identified specific behavioral and clinical factors, along with antibiotic usage, as significant contributors to such infections, potentially fostering resistant microorganisms.[34] A recent case study reported the complete regression of multifocal wart lesions in an HIV-positive patient after one session of photodynamic therapy (PDT), despite the lesion thickness. Literature reviews suggest that PDT is a viable option for immunocompromised patients at high risk of relapse.[35]

CPs exhibit potent anti-HIV activity, functioning through mechanisms such as reverse transcriptase (RT),[10,36−39] and protease inhibition.[39−42] Second-generation CPs with significant anti-HIV-1 activity have been reported[43,44] to evince HIV-1 inhibition through binding with G-quadruplex DNA. Notably, studies by Sengupta et al. revealed that CPs with *meso*-methylpyridinium and nitrophenyl groups inhibited HIV-1 entry by over 99% at micromolar concentrations.[9] This inhibitory effect extended to simian immunodeficiency virus (SIVmac), underscoring the versatility of CPs in antiviral applications.[9] Other publications on asymmetric pyridinium porphyrins have also corroborated similar findings.[10,14,43,44] The incorporation of metals, such as gold and zinc, further enhances the antiviral potential of CPs.[8,10,43,45] Amphiphilicity conferred by cationic charges improves therapeutic outcomes, encouraging the design of CPs with mixed cationic groups to optimize photobiological efficacy.[10,14,43,44]

Despite significant advancements in the development of CPs for PDT applications, a deeper exploration of the structure−activity relationships (SAR) governing their dual effectiveness against drug-resistant bacteria and viruses remains essential. This study focuses on newly synthesized porphyrins featuring combinations of cationic groups and their zinc complexes. These compounds (Figure 1), with **A_3B**, **A_2B_2**, and **AB_3** configurations of *meso*-methylpyridinium and *meso*-trimethylammonium phenyl groups, along with their zinc counterparts, represent innovative examples of simultaneous quaternariza-

https://doi.org/10.1021/acsomega.4c09535
ACS Omega 2025, 10, 22482−22507

Scheme 1. Synthetic Methodology Involved in the Synthesis of the Free-Base and Zinc-Metalated Ammonium Phenyl Porphyrins P_3AmM, P_3AmZM, c-P_2Am_2M,c-P_2AM_2ZM, PAm_3M, and PAm_3ZM

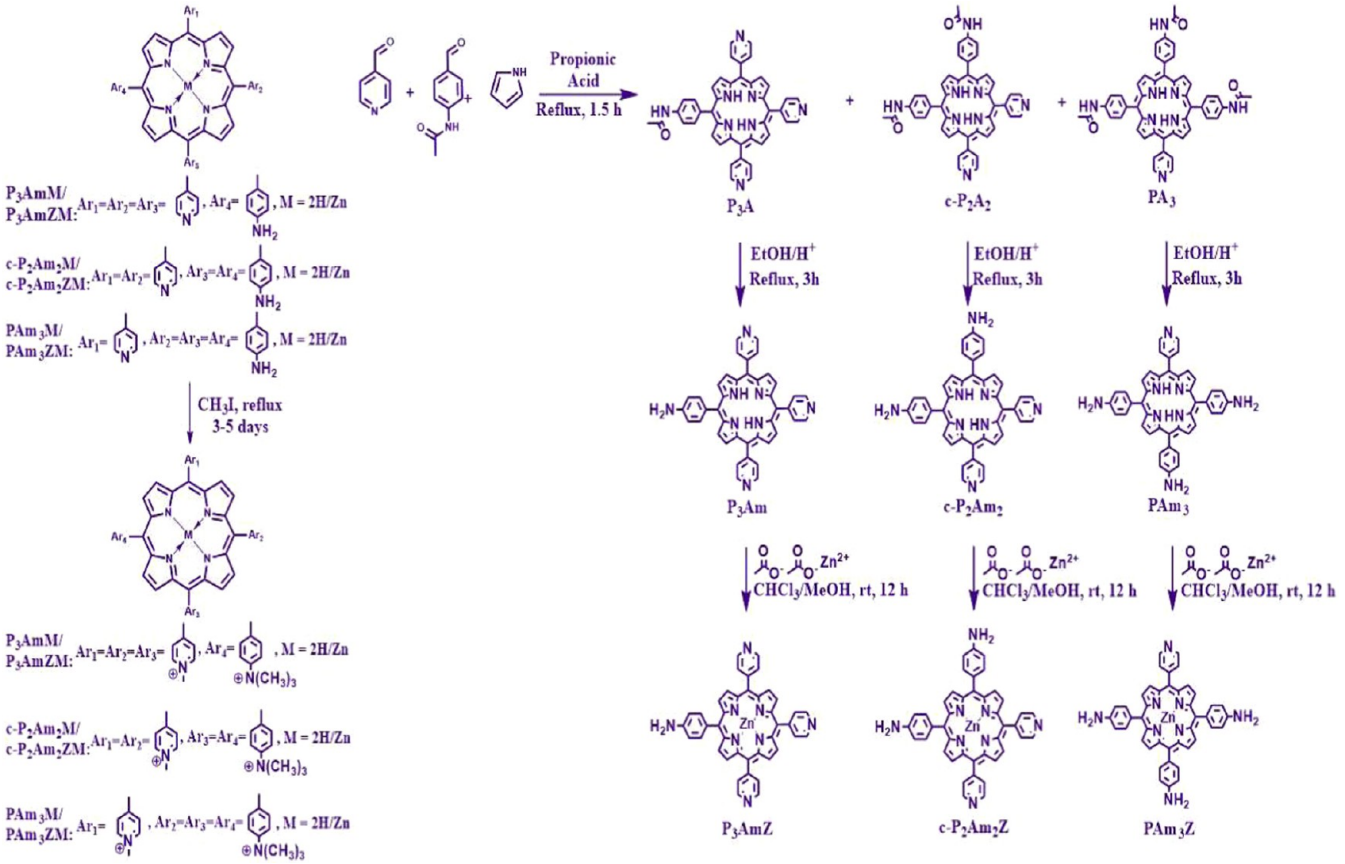

Scheme 2. Synthesis of P_3Am, c-P_2Am_2, and PAm_3

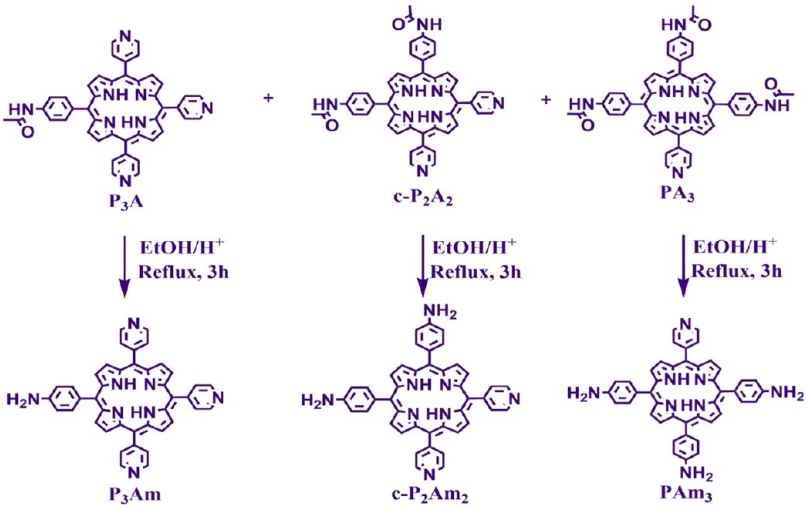

tion and methylation strategies. Such novel designs address existing limitations and pave the way for advanced photodynamic antimicrobial and antiviral therapies.

2. RESULTS AND DISCUSSION

2.1. Synthesis, Isolation, and Characterization. *2.1.1. Synthesis.* The cationic water-soluble porphyrins were synthesized through a multistep methodology as outlined in Scheme 1. A one-pot three-component reaction involving 4-acetamidobenzaldehyde (1.5 equiv), pyridine-4-carboxaldehyde (3.2 equiv), and pyrrole (4 equiv) led to the formation of the products 5,10,15-tri-(4-acetamidophenyl)-20-(4-pyridyl) porphyrin (**PA_3**), 5,10-di(4-acetamidophenyl)-15,20-di(4-pyridyl) porphyrin (**c-P_2A_2**), 5-(4-acetamidophenyl)-10,15,20-tri-(4-pyridyl) porphyrin (**P_3A**). TLC of the crude reaction mixture indicated the formation of six compounds, of which only three (**PA_3**, **c-P_2A_2** and **P_3A**) were isolated and characterized. Isolation was achieved through gravity percolation chromatography, silica gel 60−200 mesh, and (3−10%)

https://doi.org/10.1021/acsomega.4c09535
ACS Omega 2025, 10, 22482−22507

Scheme 3. Synthesis of Zn Complexes P_3AmZ, c-P_2Am_2Z, and PAm_3Z

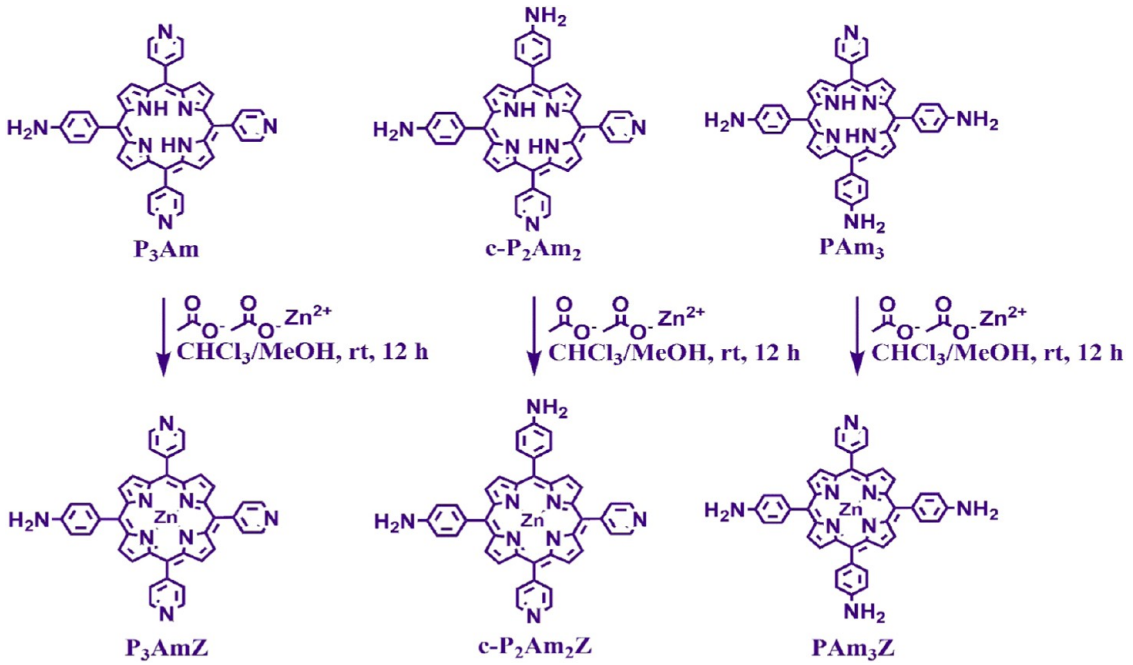

Scheme 4. Synthesis of P_3AmM, c-P_2Am_2M, PAm_3M, P_3AmZM, c-P_2Am_2ZM, and PAm_3ZM

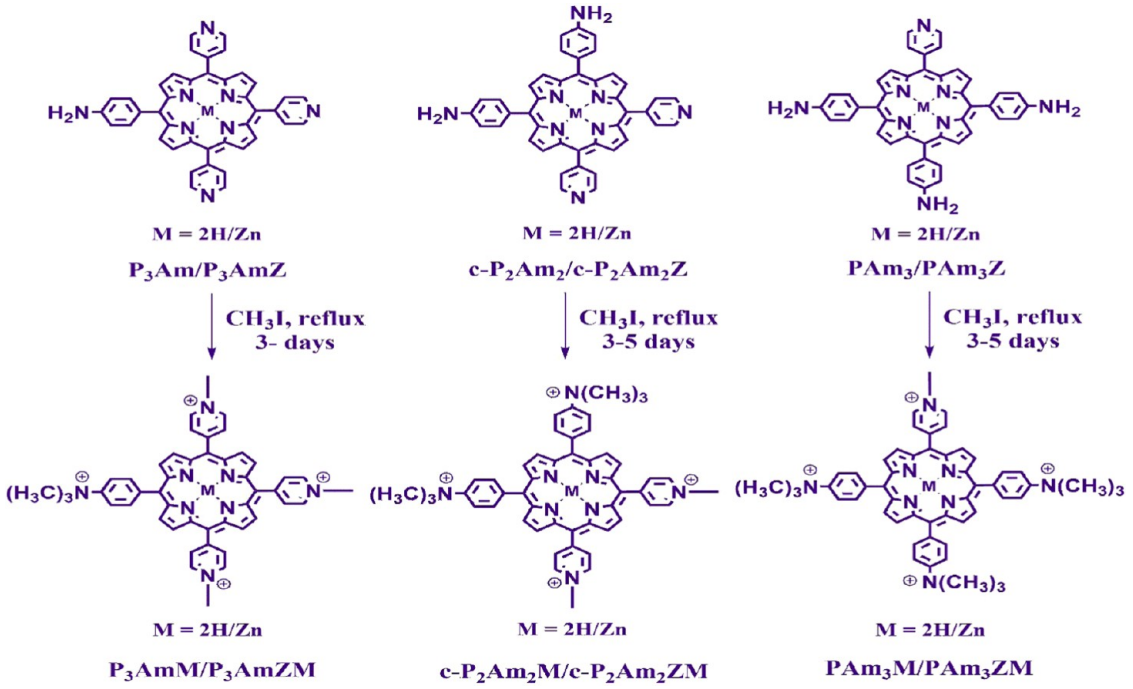

MeOH in DCM being the stationary and mobile phases, respectively. **P_3A** was the first to elute with 5% MeOH in DCM followed by **c-P_2A_2**. **PA_3** eluted out in 7% MeOH in DCM. Wherever required, a second column was run for further purification. **P_3A**, **c-P_2A_2**, and **PA_3** were obtained in 10, 9, and 6% yield. The isolation of the rest of the fractions was not attempted. The compound **P_3A** has been reported earlier, the synthesis being achieved through a protocol either similar to the one included in this paper[46] or a different one.[47,48] Compound **c-P_2A_2** has been reported earlier with a different synthetic strategy.[49] To our knowledge, **PA_3** has not been reported so far. The acetamidophenyl porphyrins were then hydrolyzed (Scheme 2) to form the corresponding *meso*-aminophenyl substituted porphyrin derivatives 5,10,15-tri-(4-aminophenyl)-20-(4-pyridyl) porphyrin (**PAm_3**), 5,10-di(4-aminophenyl)-15,20-di(4-pyridyl) porphyrin (**c-P_2Am_2**), 5-(4-aminophenyl)-10,15,20-tri-(4-pyridyl) porphyrin (**P_3Am**). As shown in Scheme 2, an ethanolic solution of **P_3A**, e.g., is reacted with HCl (5 M) under reflux conditions, and the amide bond of the lone acetamidophenyl group of the compound gets cleaved, forming an aminophenyl function as in compound **P_3Am**. **PAm_3**, **c-P_2Am_2**, and **P_3Am** were obtained in 82, 96, and 88% yield, respectively. The synthesis of **P_3Am** with the same reagent mixture but under different

https://doi.org/10.1021/acsomega.4c09535
ACS Omega 2025, 10, 22482−22507

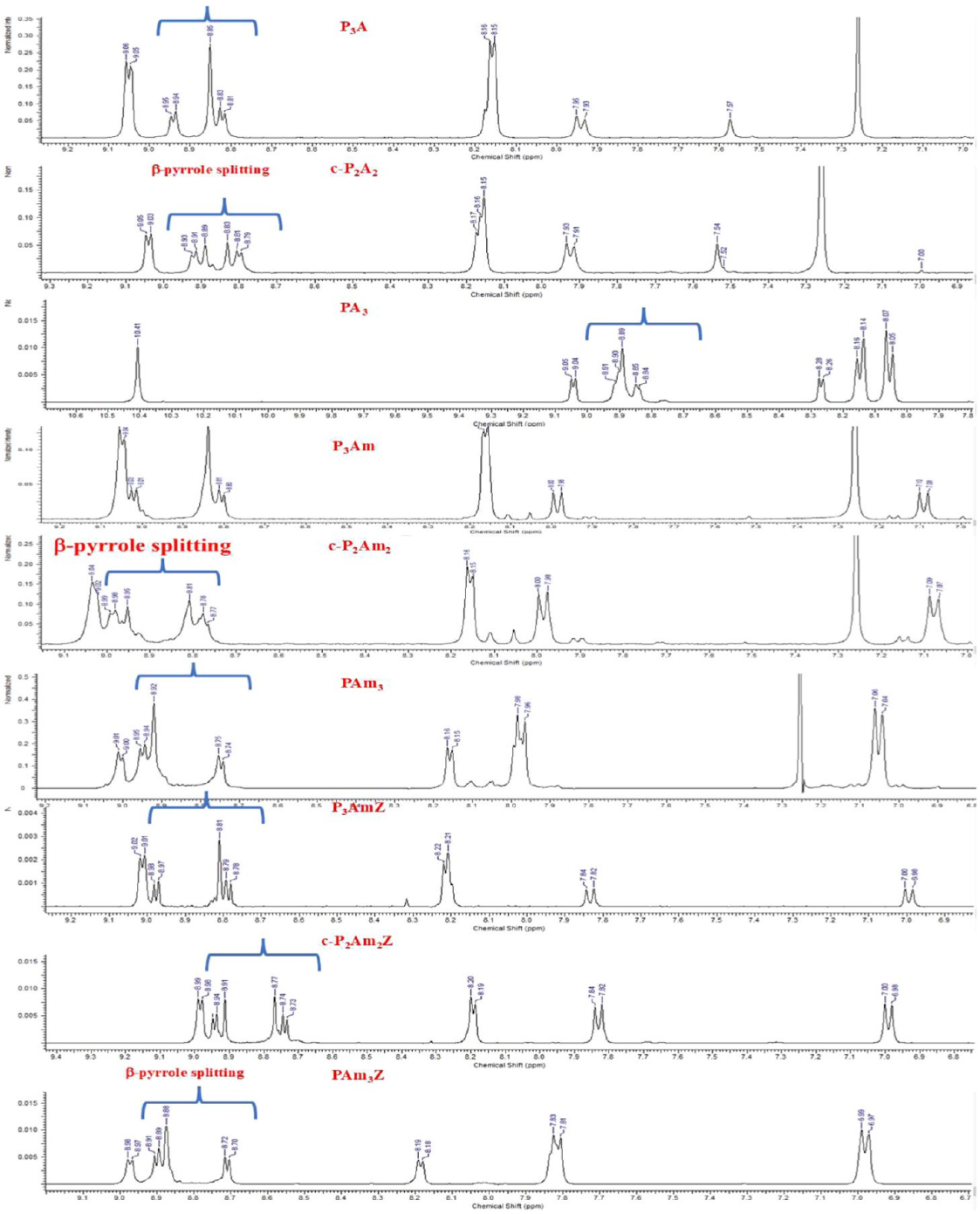

Figure 2. *β*-Pyrrole splitting in the ^{1}H NMR spectra of **P$_3$A, c-P$_2$A$_2$, PA$_3$, P$_3$Am, c-P$_2$Am$_2$, PAm$_3$, P$_3$AmZ, c-P$_2$Am$_2$Z**, and **PAm$_3$Z**. Data recorded in $CDCl_3$ for **c-P$_2$A$_2$, P$_3$Am, c-P$_2$Am$_2$**, and **PAm$_3$**. Data recorded in DMSO-d6 for **P$_3$A, PA$_3$, P$_3$AmZ, c-P$_2$Am$_2$Z**, and **PAm$_3$Z**.

conditions of reaction and workup has been reported earlier.[46,50] In contrast compounds **c-P$_2$Am$_2$** and **PAm$_3$** have been synthesized using an entirely different methodology involving a Lossen rearrangement. Derivatives of the type **CM$_x$Py$_y$P** were warmed to 100 °C in polyphosphoric acid, then gradually to 160 °C over 3 h followed by neutralization with NaOH to obtain **c-P$_2$Am$_2$** and **PAm$_3$** (or ***cis*-A$_2$Py$_2$P** and **APy$_3$P**) as reported in the publications.[47,48] Zn-metalation of the free-base porphyrins **P$_3$Am**, **c-P$_2$Am$_2$** and **PAm$_3$** was carried out by reacting the individual compounds with zinc acetate in $CHCl_3$/MeOH-9:1 v/v solution, as shown in Scheme 3. The Zn-metal complexes **P$_3$AmZ**, **c-P$_2$Am$_2$Z**, and **PAm$_3$Z** were obtained in 87, 86, and 78% yields, respectively.

The free-base porphyrins **P$_3$Am**, **c-P$_2$Am$_2$**, **PAm$_3$**, and the zinc complexes **P$_3$AmZ**, **c-P$_2$Am$_2$Z**, and **PAm$_3$Z** were then alkylated through reaction with methyl iodide under refluxing conditions to produce the hydrophilic polyiodide salts **P$_3$AmM**, **c-P$_2$Am$_2$M**, **PAm$_3$M**, and their Zn-metal complexes **P$_3$AmZM**, **c-P$_2$Am$_2$ZM**, and **PAm$_3$ZM** (Scheme 4). In each case, the alkylation of the *meso*-(4-pyridyl) groups to *meso*-(4-methylpyridinium) and *meso*-(4-aminophenyl) to *meso*-(4-trimethylammonium phenyl) moieties was achieved. This synthetic achievement results in the first-ever report of direct

https://doi.org/10.1021/acsomega.4c09535
ACS Omega 2025, 10, 22482−22507

quaternarization of *meso*-(4-aminophenyl) moieties in porphyrins bearing a combination of *meso*-(4-aminophenyl) and *meso*-(4-pyridyl) groups. The synthesized polyiodide salts were readily hydrophilic, thus rendering them useful for biochemical explorations. Alkylation involving **5-(4-aminophenyl)-10,15,20-tri-(4-pyridyl) porphyrin** attempted with a different synthetic methodology has been reported earlier.[51] Nevertheless, the authors could not achieve quaternarisation of the *meso*-(4-aminophenyl) group.

2.1.2. Characterization. The synthesized compounds were characterized using ^{1}H NMR, high-resolution mass spectrometry (electrospray ionization)/Matrix-assisted laser desorption/ionization time-of-flight (HRMS (ESI)/MALDI-TOF), ultraviolet−visible (UV−vis), and emission spectroscopic techniques. The proton splitting pattern of the synthesized compounds has been included in Table S1 for greater clarity. The splitting patterns are consistent with the A_3B/AB_3 and cis-A_2B_2 systems reported in the literature.[8,9,52−55] For compounds **P_3A**, **c-P_2A_2**, and **PA_3**, the spectral plots (Figures S5−S7) indicate that the β-pyrrole protons are split into doublet-singlet-doublet at 8.94 (d, J = 4.7 Hz)−8.85 (s)−8.82 (d, J = 4.7 Hz) ppm, 8.92 (d, J = 4.7 Hz)−8.89 (s)−8.83 (s)−8.8 (d, J = 4.7 Hz) ppm, and 8.92 (d, J = 4.2 Hz)-8.89(s)−8.84 (d, J = 4.2 Hz) ppm, respectively. The pyridyl protons resonate at 9.05 (d, J = 4.1 Hz), 8.16 (d, J = 4.1 Hz) for **P_3A**, 9.05 (d, J = 5 Hz), 8.16 (d, J = 5 Hz) for **c-P_2A_2**, and 9.04 (d, J = 4.9 Hz), 8.27 (d, J = 4.9 Hz) ppm for **PA_3**.

The proton splitting for the phenyl protons appeared at 7.94 (d, J = 7.9 Hz) and 7.56 (d, J = 7.9 Hz) for **P_3A**, 7.92 (d, J = 7.9 Hz) and 7.53 (d, J = 7.9 Hz) for **c-P_2A_2**, 8.15 (d, J = 8.1 Hz) and 8.06 (d, J = 8.1 Hz) ppm in the case of **PA_3**. The ^{1}H NMR spectral data of **P_3A** conforms to the published values.[46,50,56] For **P_3Am**, **c-P_2Am_2**, and **PAm_3**, the ^{1}H NMR spectral plots (Figures S8−S10) and tabulated spectral data (Table S1) agree with the published values[47,48] and confirm the identity of the compounds. The HRMS (ESI) data of the acetamidophenyl and aminophenyl porphyrins further indicate their purity; the mass error in each case was less than 5 ppm (Figures S20−S25). The striking feature in ^{1}H NMR spectral data (Table S1 and Figures S11−S13) of the Zn complexes is the disappearance of the highly shielded inner pyrrolic proton peak, a characteristic of the successful metalation of the porphyrins. Apart from that, the β-pyrrole splitting patterns (Figure 2) conform to that of the A_3B/AB_3 and c-A_2B_2 systems. For **P_3AmZ** and **PAm_3Z**, the β-pyrrole protons are split into doublet-singlet-doublet centered at 8.98 (d, J = 4.4 Hz)-8.81 (s)-8.79 (d, J = 4.4 Hz) and 8.9 (d, J = 4.6 Hz)-8.88 (s)-8.71 (d, J = 4.6 Hz) ppm, respectively. Proton resonances at 8.94 (d, J = 4.4 Hz)-8.91 (s)-8.77 (s)-8.74 (d, J = 4.4 Hz) ppm were observed for β pyrrolic protons of **c-P_2Am_2Z**. The pyridyl and phenyl protons are split into four doublets centered at 9.01 (d, J = 4.6 Hz), 8.21 (d, J = 4.6 Hz) and 7.83 (d, J = 8.1 Hz), 6.99 (d, J = 8.1 Hz) ppm, respectively, for **P_3Am**, 8.98 (d, J = 4.9 Hz), 8.19 (d, J = 4.9 Hz) and 7.83 (d, J = 8.1 Hz), 6.99 (d, J = 8.1 Hz) ppm, respectively for **c-P_2Am_2Z** and 8.97 (d, J = 4.9 Hz), 8.19 (d, J = 4.9 Hz) and 7.82 (d, J = 7.8 Hz), 6.98 (d, J = 7.8 Hz) ppm, respectively for **PAm_3Z**.

The amino-protons resonated as a singlet at 5.53 (s, br), 5.55 (s), and 5.48 (s) ppm for **P_3AmZ**, **c-P_2Am_2Z**, and **PAm_3Z**, respectively. The formation of the compounds was ably supported by MALDI-TOF data (Figures S26−28). The values of the observed and calculated mass were in good agreement with each other.

The alkylation of the free-base compounds and their Zn complexes was supported by the recorded MALDI-TOF (Figures S29−S34) spectra, the mass values obtained agree well with the calculated values, and the mass error is within 5 ppm limit. ^{1}H NMR (Figures S14−S19) gives further evidence in support of the alkylation, intense singlets corresponding to $-CH_3$ protons in methylpyridinium and ammonium phenyl moieties were consistently observed. However, the aromatic proton splitting presented a rather complex picture. This observation may be because of the effect of the cationic charges on electrons around the porphyrin ring. Protonation of aminophenyl porphyrins forming their ammonium phenyl counterparts has been reported to have affected ^{1}H NMR spectra.[48]

The synthesized porphyrins' UV−vis spectra (Figures S1A, S2A, and S3A) consistently depict the Soret and Q-band absorptions. Typically, these absorption spectra were recorded using a 1 μM solution of the compounds in dimethylformamide (DMF), unless otherwise specified. The absorption peaks, molar extinction coefficient, emission peaks, and Stokes shift have been included in Table S2. Minor redshifts in the absorption peaks were observed for **P_3A**, **c-P_2A_2**, and **PA_3** (Figure S1A). The emission spectra (Figure S1B) were obtained by exciting the same solutions used for the UV−vis measurements at the absorption maxima of their respective Soret bands. Emission peaks at 644, 660, and 717 nm for **P_3A**, 647, 664, and 720 nm for **c-P_2A_2** and 646, 673, and 723 nm for **PA_3** were observed.

For the aminophenyl porphyrins **P_3Am**, **c-P_2Am_2**, and **PAm_3** redshifts in Soret band absorptions were apparent (Figure S2A) as the number of *meso*-aminophenyl groups increased in the porphyrin skeleton in going from **P_3Am−c-P_2Am_2−PAm_3**, the magnitude of redshift being 6 nm in going from **P_3Am** to **c-P_2Am_2** and 5 nm between **c-P_2Am_2** and **PAm_3**. Redshifts to the tune of 20 nm can also be seen in the emission profile (Figure S2B) of compounds **P_3Am**, **c-P_2Am_2**, and **PAm_3** with a progressive increase in the number of *meso*-aminophenyl groups. The emission peaks corresponding to the Q(0,0) and Q(0,1) transitions are 653, 718 nm for **P_3Am**, 673, 723 nm for **c-P_2Am_2** and 694, 757 nm for **PAm_3**, although it should be stated that the Q(0,1) emission band is not well-defined in **c-P_2Am_2** and **PAm_3** and it appears more like a shoulder peak in the spectral plots (Figure S2B). Stokes shifts of 237, 251, and 263 nm were observed for **P_3Am**, **c-P_2Am_2**, and **PAm_3**, the values are much lower than the acetamidophenyl porphyrins with Stokes shifts of 242, 244, and 251 nm for **P_3A**, **c-P_2A_2**, and **PA_3**.

Evidence of Zn-metalation can be seen in the UV−vis spectral plot (Figure S3A). The incorporation of Zn is accompanied by the reduction in the number of Q-band absorptions from four in the free-base porphyrin to two in the metal complex. The reduction in the number of Q-band peaks in the Zn porphyrins is a direct consequence of the increased symmetry of the compounds relative to that of the free-base porphyrins. The inner pyrrolic protons in the porphyrin core reduce the symmetry from D_{4h} to D_{2h}.[57] Redshift in Soret band maxima can be seen with an increase in the number of appended aminophenyl groups. The λ_{max} of the Soret band absorption for **P_3AmZ**, **c-P_2Am_2Z**, and **PAm_3Z** are 427, 432, and 435 nm, respectively. The Q-band peaks appear at 560 and 603 nm for **P_3AmZ**, 563 and 607 nm for **c-P_2Am_2Z** and finally, 566 and 611 nm for **PAm_3Z**. A blueshift of emission maxima also accompanies complex formation (Figure S3B); the

https://doi.org/10.1021/acsomega.4c09535
ACS Omega 2025, 10, 22482−22507

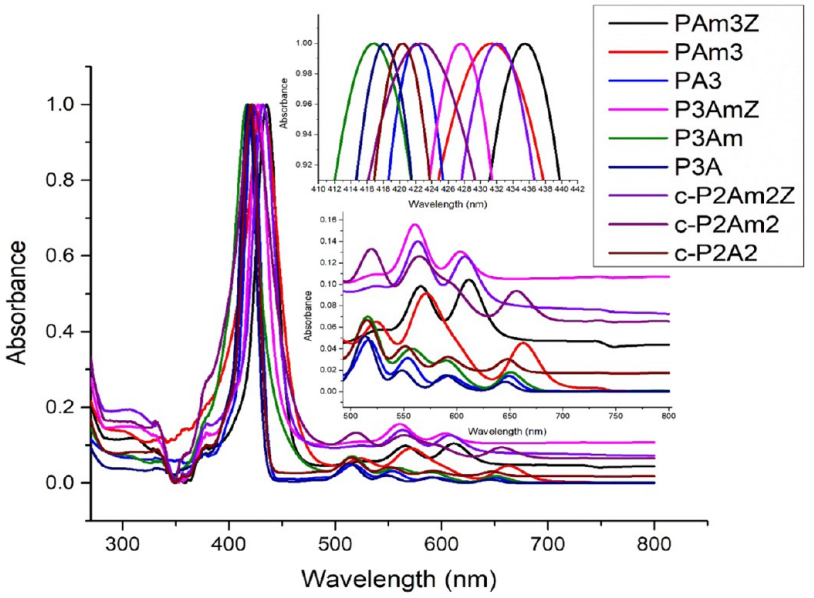

Figure 3. Comparative UV−vis plot of **P_3A, P_3Am, P_3AmZ, c-P_2A_2,** c-**P_2Am_2, c-P_2Am_2Z, PA_3, PAm_3,** and **PAm_3Z,** spectral data recorded in DMF at a concentration of 1 μM.

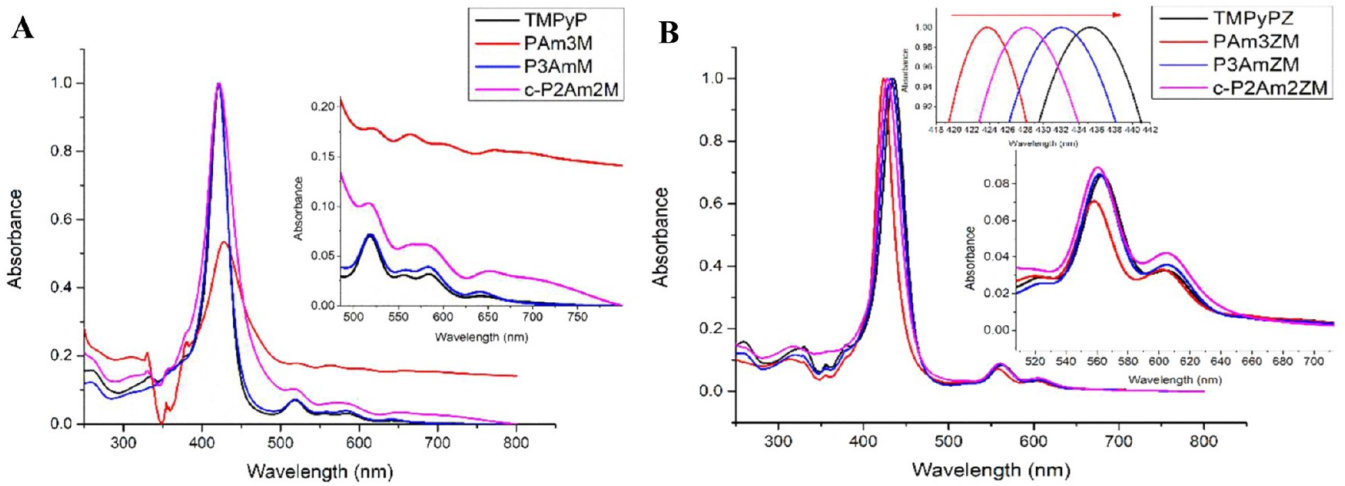

Figure 4. (A) Comparative UV−vis's plot of **TMPyP**, **PAm_3M**, **c-P_2Am_2M**, and **P_3AmM** and (B) Comparative UV−vis's plot of **TMPyPZ**, **PAm_3ZM**, **c-P_2Am_2ZM**, and **P_3AmZM**, spectral data recorded in water at a concentration of 10 μM.

compounds also show a blue shift in Q(0,0) emission peaks with a progressive reduction in the number of *meso*-aminophenyl groups from three in **PAm_3Z** to two in **c-P_2Am_2Z** and to just one in **P_3AmZ**. Blueshifts were also observed in the Q(0,1) emission band with a reduction in the number of *meso*-aminophenyl groups. However, the trend is different, with the observed blue shift being highest for **c-P_2Am_2Z**.

The comparative UV−vis plot of the compounds (Figure 3) clearly shows a blue shit in Soret band absorption of the *meso*-acetamidophenyl porphyrins upon hydrolysis to *meso*-aminophenyl porphyrins. Zn-metalation of the latter was accompanied by a significant red shift in λ_{max} of the Soret band. Table S2 includes the detailed UV−vis and emission data of **P_3A, c-P_2A_2, PA_3, P_3Am, c-P_2Am_2, PAm_3, P_3AmZ, c-P_2Am_2Z,** and **PAm_3Z** with calculated Stokes shift and molar extinction coefficient for better clarity. The magnitude of Stokes shift for the free-base acetamidophenyl porphyrins is lower than the corresponding amino-porphyrins. The observed Stokes shift for the Zn complexes is much lower than their free-base counterparts.

Such a decrease of Stokes shift in Zn complexes relative to the free-base system was reported earlier[58,59] and can be attributed to the Zn-compounds taking on a more coplanar configuration in the first excited state than in the ground state.[58] Between the acetamidophenyl porphyrins and their hydrolysis products, the *meso*-(4-aminophenyl) groups probably induces more significant structural distortions on photoexcitation and, thus, the larger values of Stokes shift.

The UV−vis spectra of the CPs were recorded with a 10 μM solution of the compounds in water. The spectral plot and data are presented in Figure 4 and Table S3. The absorption spectra of the free-base CPs conform to the typical porphyrinic spectra exhibiting an intense Soret band and four Q-band absorptions. The Soret band peaks are red-shifted in the Zn complexes compared to their free-base counterpart. The number of Q-bands in the zinc complexes is also reduced to two. The

https://doi.org/10.1021/acsomega.4c09535
ACS Omega 2025, 10, 22482−22507

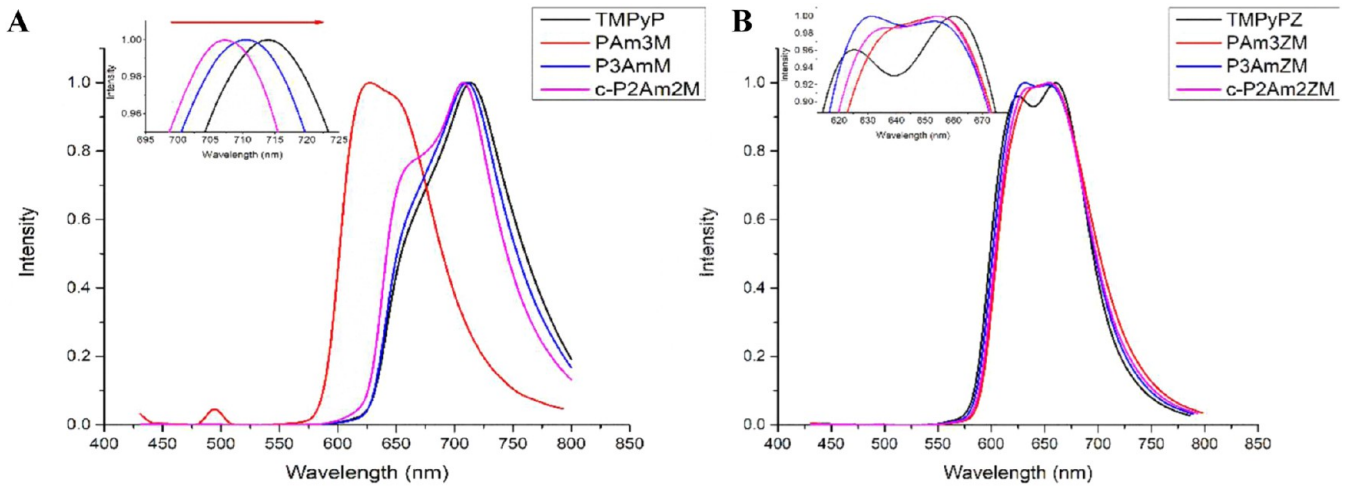

Figure 5. (A) Comparative emission plot of **TMPyP**, **PAm$_3$M**, **c-P$_2$Am$_2$M**, and **P$_3$AmM** and (B) Comparative emission plot of **TMPyPZ**, **PAm$_3$ZM**, **c-P$_2$Am$_2$ZM**, and **P$_3$AmZM**, spectral data recorded in water at a concentration of 10 μM.

observed spectral behavior is in agreement with Gouterman's model.[60]

A progressive red shift in the Soret band is also apparent in going from **PAm$_3$ZM-c-P$_2$Am$_2$ZM-P$_3$AmZM-TMPyPZ** (Figure 4A). The emission spectra (Figure 5) of the ammonium phenyl porphyrins shows variable results. The spectral data were recorded by excitation of a 10 μM solution of the compounds in water at the λ_{max} of their Soret bands. While emission peaks pertaining to the Q(0,0) and Q(0,1) emission bands can be observed for **P$_3$AmZM**, **c-P$_2$Am$_2$ZM** with emission peaks at 630, 653 nm and 634, 654 nm, respectively, the two peaks appear to have merged for **PAm$_3$ZM** with a maximum at 657 nm. The free-base CP **c-P$_2$Am$_2$M** also exhibits two emission bands at 658 and 710 nm. For **P$_3$AmM** a single emission band could be observed with a maxima at 623 nm, whereas for **PAm$_3$M** emission peaks appeared at 658 and 707 nm. The UV−vis, emission spectral data, and molar extinction coefficient have been included in Table S3. A blue shift in emission peak maxima is apparent on Zn-complexation; however, the emission maxima of **P$_3$AmM** was blue-shifted by 10 nm compared to its Zn-complex **P$_3$AmZM**. The Stokes shift calculated[61,62] presented interesting outcomes (Table S3). The large values indicate structural changes upon photoexcitation.[58,63,64] The Stokes shift values for the free-base porphyrins were more prominent than their Zn complexes, **PAm$_3$M** and **PAm$_3$ZM** being exceptions here. This agrees with earlier reports,[58,59] and indicates that the Zn complexes take on a more planar configuration in the first excited state than in the ground state compared to the free-base compounds.[58,64] The large values of Stokes shift also mean reduced homo-FRET and consequently minimal self-quenching.[65,66] This is desirable as far as the applications of the CPs as PSs are concerned.

To assess the fluorescence quantum yields (Φ_f) of the hydrophilic compounds detailed in Table 1, each compound was tested at a uniform concentration of 10 μM in water. **TCPP** in ethanol, with a reported Φ_f value of 0.044,[67] served as the reference standard for these measurements. The calculation of Φ_f was carried out using the following equation

$$\Phi_f = \Phi_{f_{std}} \frac{I(1-10^{-A})_{std}\eta^2}{I_{std}(1-10^{-A})\eta_{std}^2}$$

Table 1. Fluorescence Quantum Yield of P$_3$AmM, c-P$_2$Am$_2$M, PAm$_3$M, P$_3$AmZM, c-P$_2$Am$_2$ZM, PAm$_3$ZM, TMPyP, and TMPyPZ Recorded in Water at a Concentration of 10 μM

compound	fluorescence quantum yield Φ_f
P$_3$AmM	0.032
c-P$_2$Am$_2$M	0.013
PAm$_3$M	0.004
P$_3$AmZM	0.034
c-P$_2$Am$_2$ZM	0.030
PAm$_3$ZM	0.037
TMPyP	0.044
TMPyPZ	0.036

Here, Φ_f represents the fluorescence quantum yield, I is the integrated fluorescence intensity, A is the absorbance at the excitation wavelength, and η denotes the refractive index of the solvent (with values of 1.333 for water and 1.3614 for ethanol). The subscript "std" refers to the standard compound, in this case, **TCPP**. The data revealed that **TMPyP** had the highest Φ_f (0.044) among the compounds tested. This finding aligns with previous studies on **TMPyP**.[68,69] Generally, the zinc complexes of the hydrophilic porphyrins exhibited higher Φ_f values, except for **TMPyPZ**, which had a lower Φ_f (0.036) compared to its free-base counterpart **TMPyP**. For the free-base compounds, the calculated Φ_f values are 0.032, 0.013, and 0.004 for **P$_3$AmM**, **c-P$_2$Am$_2$M**, and **PAm$_3$M**. The zinc complexes **P$_3$AmZM**, **c-P$_2$Am$_2$ZM**, and **PAm$_3$ZM** exhibited Φ_f values of 0.034, 0.030, and 0.037.

The efficient generation of singlet oxygen by PSs is considered a benchmark of their photodynamic efficacy. As such, the quantum yield of singlet oxygen generation (Φ_Δ) for the target PSs was determined through the photooxidation of 9,10-dimethylanthracene (DMA),[70−72] In a typical experimental setup, the time-dependent decrease in absorbance of DMA was monitored separately in the presence of the compounds **P$_3$AmM**, **c-P$_2$Am$_2$M**, **PAm$_3$M**, **P$_3$AmZM**, **c-P$_2$Am$_2$ZM**, and **PAm$_3$ZM**. The reaction follows pseudo-first-order kinetics. To determine the rate constant (k) for each PS, a graph of $\ln(A_0/A)$ against the irradiation time in minutes was used. The rate equation governing this process is provided in eq 1

https://doi.org/10.1021/acsomega.4c09535
ACS Omega 2025, 10, 22482−22507

$$\ln\left(\frac{A_o}{A}\right) = kt \quad (1)$$

Here, 'A_0' is the initial absorbance of the PSs, 'A' is the absorbance at any given irradiation time, 'k' represents the first-order rate constant, and 't' is the irradiation time. The obtained

Table 2. Rate Constant (k) for the Photooxidation of DMA in DMF by P_3AmM, c-P_2Am_2M, PAm_3M, P_3AmZM, c-P_2Am_2ZM, PAm_3ZM, and their Respective Singlet Oxygen Quantum Yield ($\Phi\Delta$)

	rate constant (k) min^{-1}	
compound	Φ_f	singlet oxygen quantum yield
c-P_2Am_2ZM	0.00438	0.73
c-P_2Am_2M	0.00673	0.68
PAm_3M	0.00846	0.30
P_3AmM	0.00974	0.48
PAm_3ZM	0.01186	0.51
P_3AmZM	0.01244	0.64

k values (see Table 2) were further utilized to calculate the Φ_Δ of the target PSs using eq 2

$$\Phi_\Delta = \Phi_{\Delta(ref)}\frac{A \times k_{ref}}{A_{ref} \times k} \quad (2)$$

In this equation, Φ_Δ and $\Phi_{\Delta(ref)}$ denote the singlet oxygen quantum yields of the PSs and the reference compound **H_2TPP**, respectively. 'A' and 'A_{ref}' are the absorbance values for the PSs and the reference compound **H_2TPP**, while 'k' and 'k_{ref}' represent the rate constants derived from the photooxidation kinetics of DMA by the PSs and **H_2TPP**, respectively. All experiments were conducted in DMF, with **H_2TPP** (Φ_Δ = 0.64 in DMF) used as the reference standard.[72] Among the compounds **c-P_2Am_2ZM** exhibited the highest Φ_Δ = 0.73 and **PAm_3M** the lowest Φ_Δ (0.30). For other compounds, the observed values ranged between 0.50 to 0.70. As a general trend, the Zn complexes had higher Φ_Δ compared to their free-base counterparts.

2.2. Anti-HIV Activity. In the present study, the anti-HIV activities of cationic ammonium phenyl porphyrins are reported. The anti-HIV activity was tested using several biochemical and virological assays under both nonphotodynamic (non-PDT) and photodynamic conditions (PDT) as described.

2.2.1. Ammonium Phenyl Porphyrins were not Cytotoxic under Non-PDT or PDT Conditions. The effect of ammonium phenyl porphyrins on the viability of HEK-293T and TZM-bl cells was determined using Cell Titer-Blue Assay under non-PDT and PDT conditions as described in the methods. None of the porphyrins were toxic to the cells at the concentrations tested in non-PDT conditions from 0.1 to 10 μM. The half-maximal cytotoxic concentrations (CC_{50} value) determined were greater than 10 μM (Table S4). Hence, for further experiments under non-PDT conditions, porphyrins were used at 5 μM. Under PDT conditions as described in methods, cell viability was determined in the presence of porphyrins at concentrations from 0.1 to 0.5 μM. Again, all the porphyrins were nontoxic to cells under PDT conditions with half-maximal cytotoxic concentrations (CC_{50} value) of >500 nM. Hence, porphyrins were used at 500 nM for further experiments under PDT conditions.

2.2.2. Ammonium Phenyl Porphyrins Reduced Virus Infectivity under Non-PDT Conditions. The infectivity of the viruses produced in the presence of compounds was analyzed by using a TZM-bl cell-based single-cycle infectivity assay[73,74] as described in the methods. Briefly, HEK-293T cells were transfected with pNL4−3 subtype B virus and incubated with porphyrins at a concentration of 5 μM for 24 h. The amount of virus released in the supernatant was quantified by p24 ELISA. Then, TZM-bl cells were infected with 10 ng of HIV-1 p24 equiv NL4−3 virus for 2 h. The cells were washed postinfection and incubated in fresh media further for 48 h. Relative luminescence was measured 48 h postinfection and was compared to the control (−). Control refers to the HIV-1 subtype B NL4−3 virus produced with 5% DMSO in water in the absence of porphyrins. It was observed that the porphyrins containing three ammonium phenyl moieties and single pyridinium and its Zinc derivative- **PAm_3M** and **PAm_3ZM** reduced virus infectivity by 30 and 80%, respectively. Zinc metalation of **PAm_3M** enhanced its antiviral activity robustly. Similarly, zinc−metalated **TMPyPZ** exhibited a significant reduction in virus infectivity by 75% compared to its precursor **TMPyP** by only 30% (Figure 6A). Hence, it was evident that the incorporation of zinc in these structures enhanced their antiviral activity. Both **c-P_2Am_2M** and its zinc derivative **c-P_2Am_2ZM** containing two ammonium phenyl moieties and two pyridinium were most effective in reducing virus infectivity by 96% irrespective of zinc metalation. Further, in the case of **P_3AmM**, containing three pyridinium moieties and a single ammonium phenyl group, the reduction in infectivity was 80% but was reduced to 40% inhibition on the addition of zinc in **P_3AmZM**. These results suggested that the presence of two ammonium phenyl moieties linked to two pyridinium groups exhibited the most potent antiviral activity.

2.2.3. Ammonium Phenyl Porphyrins Inhibited HIV-1 Production Postentry under Non-PDT Conditions. Viral entry inhibition, an early step in the virus life cycle, was then determined in the presence of ammonium phenyl porphyrins. Inhibition assays were performed in TZM-bl cells as described in the methods. Briefly, TZM-bl cells were infected with 10 ng of HIV-1 p24 equiv subtype B NL4−3 virus, and porphyrins at 5 μM were added during virus infection as explained in methods.

The reference porphyrins **TMPyP** and **TMPyPZ** were used as a control as they have been reported to show anti-HIV activity.[10,69] Enfuvirtide (T20), a known HIV-1 fusion inhibitor was used as a positive control.[75] **c-P_2Am_2M**, **P_3AmM**, and **PAm_3ZM**, restricted virus entry by 30%, when added during virus infection, whereas **TMPyP** and **TMPyPZ** restricted HIV-1 entry by just 20% (Figure 6B, blue bars). But **c-P_2Am_2ZM**, **P_3AmZM**, and **PAm_3M** were completely ineffective. These results show that ammonium phenyl porphyrins exhibited weak activity inhibiting HIV entry under non-PDT conditions.

Next, we wanted to test the effect of these porphyrins on HIV-1 production if added after virus entry in cells. Briefly, TZM-bl cells were first infected with HIV-1 subtype B NL4−3 virus and then incubated with porphyrins for 48 h at 37 °C as described in the methods.

We observed **c-P_2Am_2ZM**, **P_3AmM**, **PAm_3ZM**, and **TMPyPZ** showed 50, 36, 36, and 42% reduction in virus production respectively (Figure 6B, yellow bars). It was observed that the porphyrin combination **c-P_2Am_2ZM**, bearing two ammonium phenyl and two pyridinium moieties

https://doi.org/10.1021/acsomega.4c09535
ACS Omega 2025, 10, 22482−22507

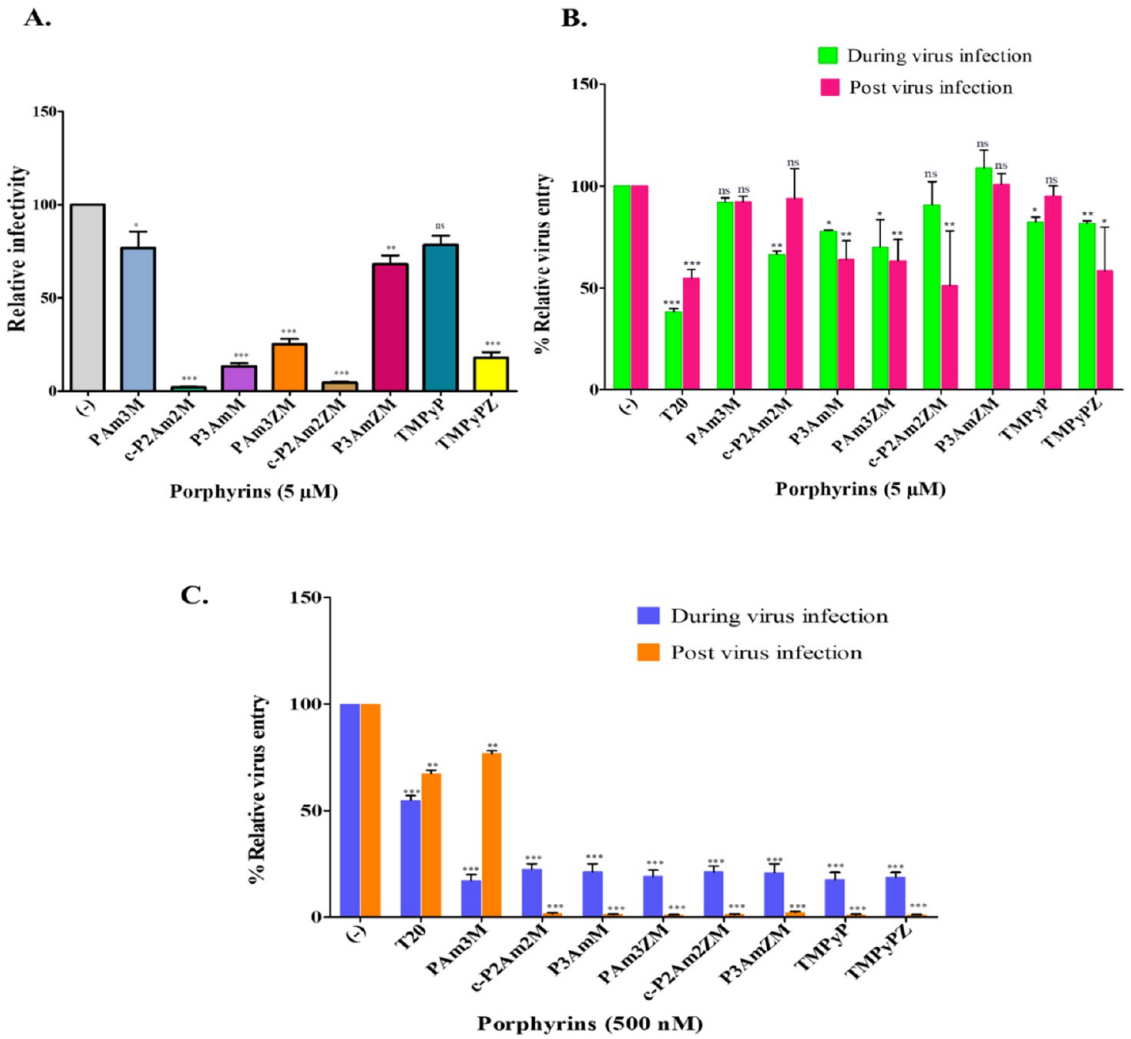

Figure 6. Aminophenyl porphyrins showed anti-HIV-1 activity in both non-PDT and PDT conditions. (A) Relative infectivity of the virus produced in the presence of 5 μM porphyrins is shown. HEK-293T cells were transfected with HIV-1 subtype B NL4−3 virus in non-PDT conditions and incubated with porphyrins for 24 h. The released virus was quantified and used to infect TZM-bl cells. Relative luciferase activity was measured. Quantitative data for levels of infectivity relative to the DMSO-water (−) control sample is shown. (B) HIV-1 subtype B NL4−3 virus entry inhibition assay in TZM-bl cells. 5 μM porphyrins were added either during the viral infection (pretreatment of virus) (blue bars) or postviral infection (yellow bars) in non-PDT conditions. (C) HIV-1 subtype B NL4−3 virus entry inhibition assay in TZM-bl cells in PDT conditions. HIV-1 subtype B NL4−3 virus was either pretreated with 500 nM porphyrins and exposed to light under PDT conditions (Blue bars), and then used to infect TZM-bl cells, the calculated light dosage at the surface is 250 J cm^{-2}, or the porphyrins were added postviral infection and exposed to light in PDT conditions (orange bars). Relative luciferase activity was measured and compared with DMSO-water (−) control. Error bars indicate standard deviations from three independent experiments. *p-value <0.05 **p-value <0.01 ***p value <0.001: student's t test.

complexed with zinc, showed maximum reduction in virus production when added postentry. Also, all porphyrins metalated with zinc were more effective than their precursor porphyrin except **P_3AmM**. These results showed that the amino-porphyrins may inhibit postentry stages of HIV infection and reduce HIV production in infected cells under non-PDT conditions.

2.2.4. Ammonium Phenyl Porphyrins Strongly Inhibited HIV-1 Entry under PDT Conditions. We next tested the effect of porphyrins on virus entry under PDT conditions as described in the methods. Briefly,10 ng of HIV-1 p24 equiv subtype B NL4−3 virus (subtype B) was preincubated with the porphyrins under PDT conditions. The experiments were carried out with the help of a custom-made irradiation box of length 20″, width 6″, and height 8″, equipped with two Philips Essential Master PL-L 36W/865/4P linear compact fluorescent lamp[8,9,76] in a way that the surface of a 96-well microplate is at a distance of 15 cm from the light source. The calculated light dosage at the surface was 250 J cm^{-2}. The pretreated virus was used to infect TZM-bl cells. Infected cells were washed and incubated for 48 h at 37 °C. Relative luciferase activity was determined with respect to control (−). Here, control refers to cells infected with a virus treated with 5% DMSO in water in the absence of porphyrins. **TMPyP** and **TMPyPZ** were used as a reference control for porphyrins known for anti-HIV activity in PDT conditions.[10,77] Enfuvirtide (T20), a known HIV-1 fusion inhibitor, was used as a positive control.[75] It was observed that pretreatment of HIV-1 subtype B NL4−3 virus with porphyrins before infection under PDT conditions blocked virus entry by more than 80% in TZM-bl cells (Figure 6C, blue bars). **PAm_3M** and **PAm_3ZM** restricted virus entry by 86 and 84% respectively whereas **c-P_2Am_2M** and **c-P_2Am_2ZM** showed 80 and 82% restriction, respectively. **P_3AmM** and **P_3AmZM** showed inhibition in virus entry by 83%. **TMPyP**

https://doi.org/10.1021/acsomega.4c09535
ACS Omega 2025, 10, 22482−22507

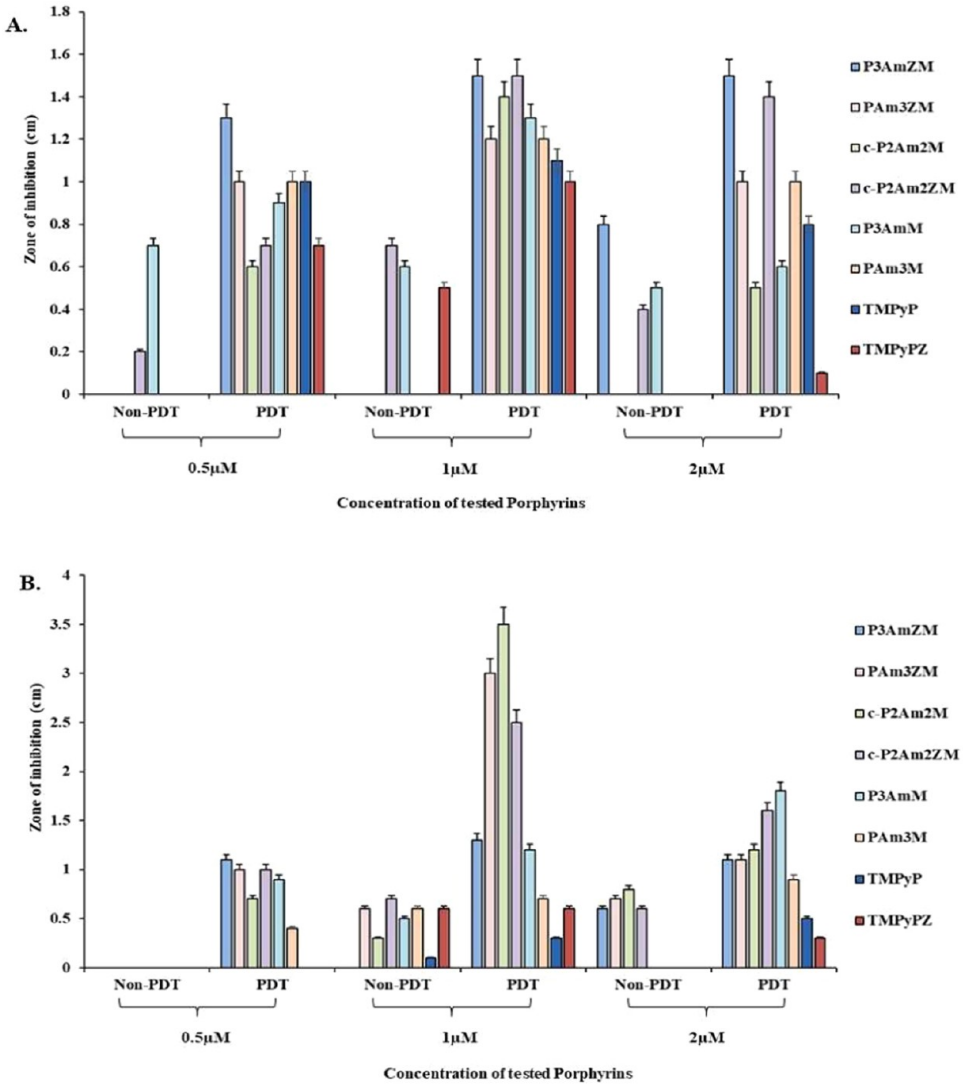

Figure 7. Cationic porphyrin compounds showed antimicrobial activity against pathogenic microbial strains (A) zone of inhibition produced during the disc diffusion method by *E. coli* ATCC 25922 and (B) zone of inhibition produced during the disc diffusion method by *S. aureus* ATCC 25923.

and **TMPyPZ** reduced virus entry by 85%. Furthermore, the addition of porphyrins postviral entry completely blocked HIV production in infected cells except **PAm$_3$M** in PDT conditions. (Figure 6C, orange bars). These results suggested that the porphyrins were potent anti-HIV agents in the presence of light (PDT) as compared to non-PDT conditions. Under PDT conditions, their activity was independent of the different combinations of ammonium phenyl group and pyridinium group or the presence/absence of zinc. Since the antiviral activity of these compounds was dependent upon light exposure, they may act as strong photosensitizers against HIV-1.

2.3. Antibacterial Activity. *2.3.1. Assessment of Antibacterial Activity through the Disc Diffusion Experiment.* The study assessed the antimicrobial efficacy of cationic ammonium phenyl porphyrins against Gram-negative *E. coli* and *S. aureus* under both nonphotodynamic (non-PDT) and photodynamic (PDT) conditions, using three different concentrations (0.5, 1, and 2 μM) (Supporting Information: Tables S5 and S6).

The photodynamic inactivation experiments were carried out with the help of a custom-made irradiation box of length 20″, width 6″, and height 8″, equipped with two Philips Essential Master PL-L 36*W*/865/4P linear compact fluorescent lamp[8,9,76] in a way that the surface of a 96-well microplate is at a distance of 15 cm from the light source. The calculated light dosage at the surface was 250 J cm^{-2}. **P$_3$AmZM** and **c-P$_2$Am$_2$ZM** demonstrated the most effective antimicrobial activity against *E. coli* under PDT conditions, with inhibition zones measuring 1.5 cm at both 1 and 2 μM concentrations. In the absence of light, **PAm$_3$M** and **PAm$_3$ZM** showed significant efficacy, producing inhibition zones of 1 and 1.2 cm, respectively, at a 1 μM concentration. c-**P$_2$Am$_2$M** exhibited the highest antibacterial activity at a 1 μM concentration under PDT conditions. Similarly, at 1 μM concentration, **P$_3$AmM** and **TMPyP** resulted in inhibition zones of 1.2 and 1.1 cm, respectively. However, **TMPyPZ** displayed lower antibacterial activity (Photoplate S1, Table S5, and Figure 7A).

Previous studies indicated that lower concentrations of the compounds resulted in weaker associations with bacterial cells, while higher concentrations led to aggregations that prevented

https://doi.org/10.1021/acsomega.4c09535
ACS Omega 2025, 10, 22482−22507

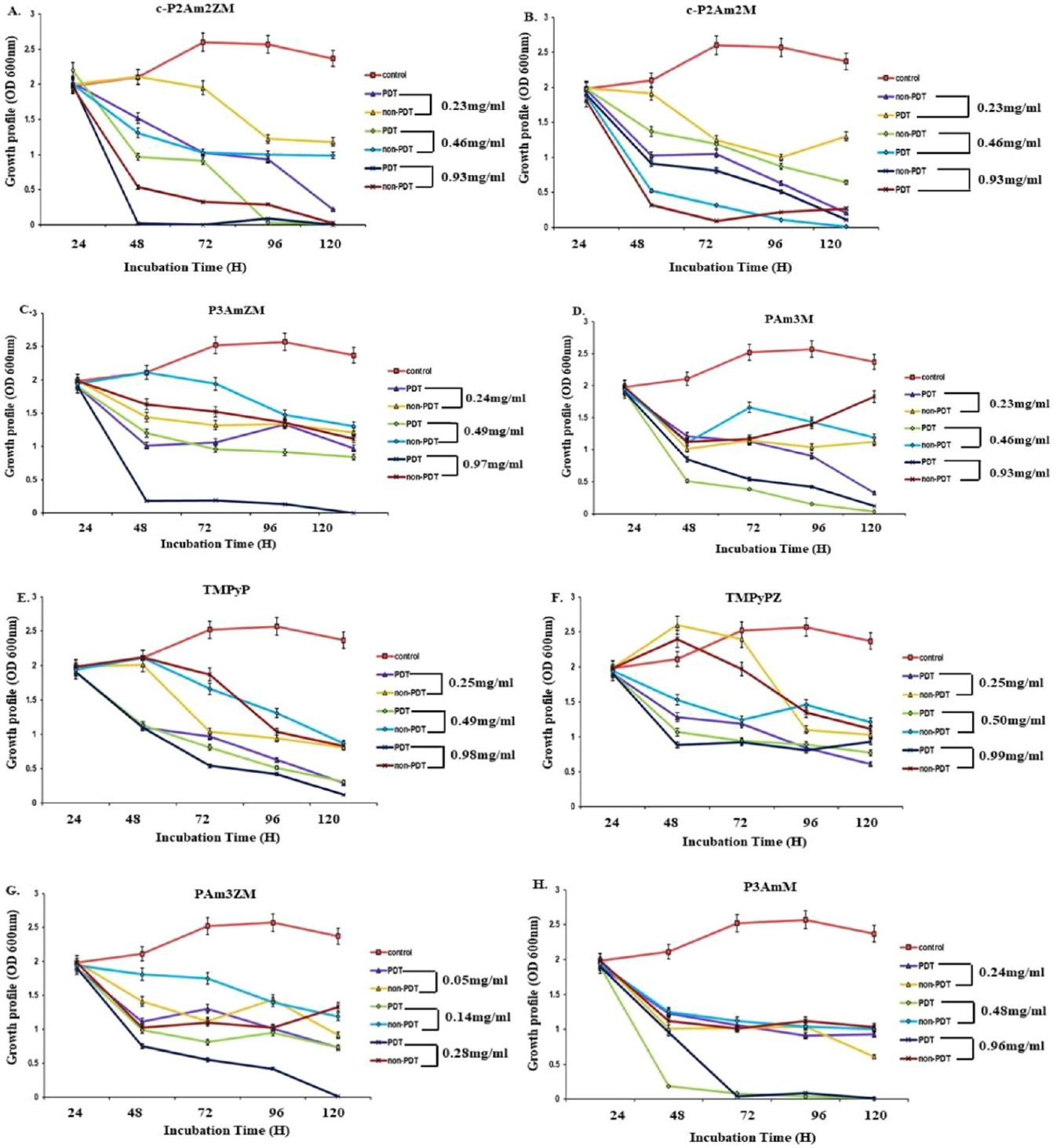

Figure 8. (A, B) Growth profile of *E. coli* for 5 days in the presence of **c-P_2Am_2ZM** and **c-P_2Am_2M** compounds in different concentrations in both PDT and non-PDT conditions. (C, D) Growth profile of *E. coli* for 5 days in the presence of **P_3AmZM** and **PAm_3M** compounds in different concentrations in both PDT and non-PDT conditions. (E, F) Growth profile of *E. coli* for 5 days in the presence of **TMPyP** and **TMPyPZ** compounds in different concentrations in both PDT and non-PDT conditions. (G, H) Growth profile of *E. coli* for 5 days in the presence of **PAm_3ZM** and **P_3AmM** compounds in different concentrations in both PDT and non-PDT conditions.

interaction with the bacterial cell wall. Therefore, an optimal moderate concentration was recommended for maximum inhibition of bacterial cells.

The susceptibility of *S. aureus* to the porphyrin compounds was notably higher. Under non-PDT conditions, c-**P_2Am_2M** and **PAm_3ZM** exhibited significant inhibition zones, measuring 3.5 and 3 cm, respectively. Under PDT conditions, c-**P_2Am_2ZM** and **P_3AmZM** showed increased antibacterial activity at 1 μM concentrations, with **P_3AmM** resulting in a 1.2 cm inhibition zone. However, **PAm_3M**, **TMPyP**, and **TMPyPZ** exhibited lower antibacterial activity against *S. aureus* in both PDT and non-PDT conditions. At 2 μM concentrations, antibacterial activity decreased, suggesting that aggregation inhibited compound activity at high concen-

https://doi.org/10.1021/acsomega.4c09535
ACS Omega 2025, 10, 22482−22507

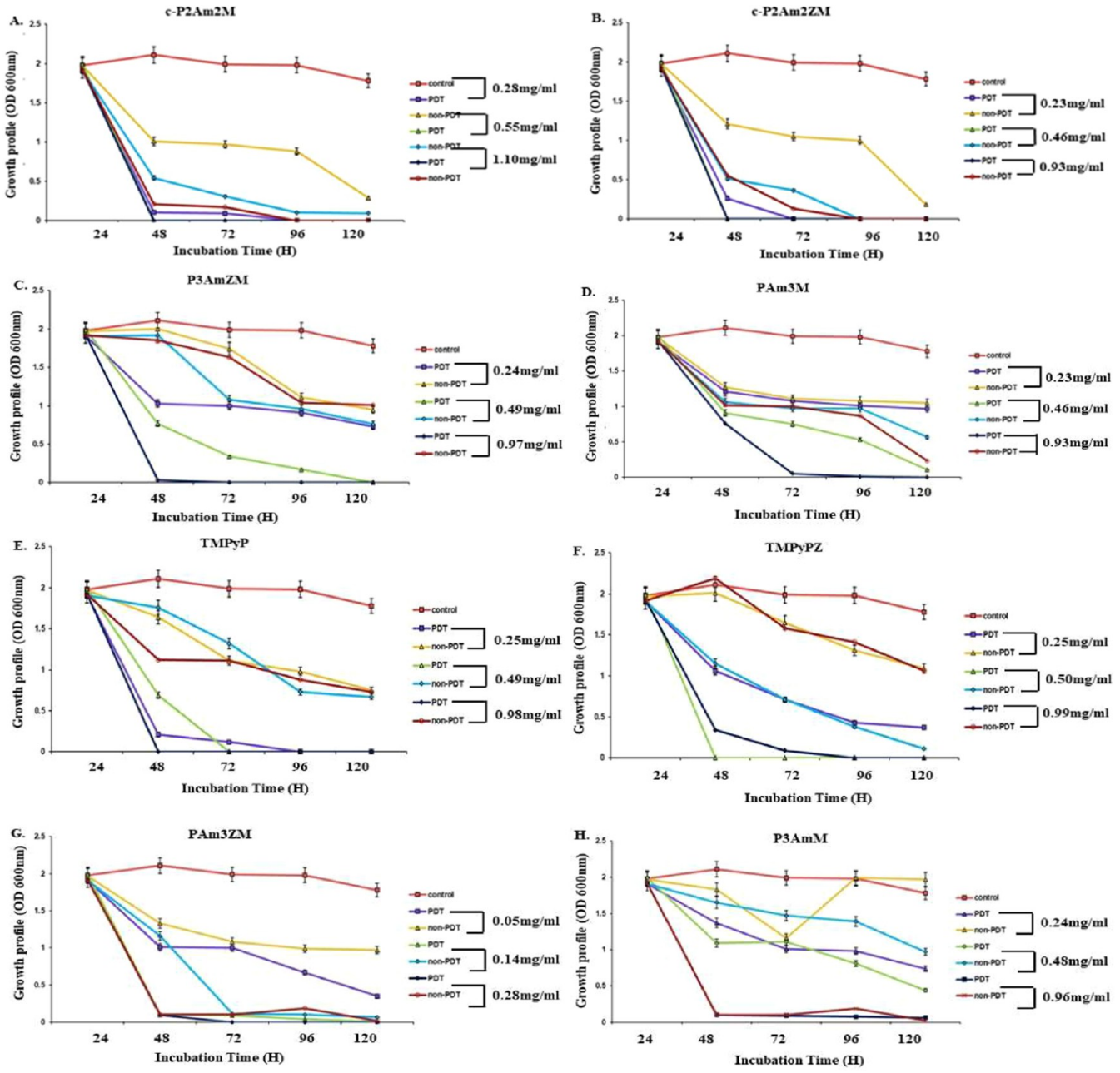

Figure 9. (A, B) Growth profile of *S. aureus* for 5 days in the presence of **c-P_2Am_2ZM** and **c-P_2Am_2M** compounds in different concentrations in both PDT and non-PDT conditions. (C, D) Growth profile of *S. aureus* for 5 days in the presence of **P_3AmZM** and **PAm_3M** compounds in different concentrations in both PDT and non-PDT conditions. (E, F) Growth profile of *S. aureus* for 5 days in the presence of **TMPyP** and **TMPyPZ** compounds in different concentrations in both PDT and non-PDT conditions. (G, H) Growth profile of *S. aureus* for 5 days in the presence of **PAm_3ZM** and **P_3AmM** compounds in different concentrations in both PDT and non-PDT conditions.

trations (Photoplate S1, Table S6, and Figure 7B). The findings demonstrate that, under PDT conditions, **P_3AmZM** and c-**P_2Am_2ZM** were the most effective compounds against *E. coli*, and *S. aureus*, followed by **P_3AmM, c-P_2Am_2M, PAm_3ZM, PAm_3M, TMPyP**, and **TMPyPZ.**

The photodynamic inactivation experiments were carried out with the help of a custom-made irradiation box of length 20″, width 6″, and height 8″, equipped with two Philips Essential Master PL-L 36*W*/865/4P linear compact fluorescent lamp[8,9,76] in a way that the surface of a 96-well microplate is at a distance of 15 cm from the light source. The calculated light dosage at the surface was 250 J cm^{-2}. **P_3AmZM** and **c-P_2Am_2ZM** demonstrated the most effective antimicrobial activity against *E. coli* under PDT conditions, with inhibition zones measuring 1.5 cm at both 1 and 2 μM concentrations. In the absence of light, **PAm_3M** and **PAm_3ZM** showed significant efficacy, producing inhibition zones of 1 and 1.2 cm, respectively, at a 1 μM concentration. c-**P_2Am_2M** exhibited the highest antibacterial activity at a 1 μM concentration under PDT conditions. Similarly, at 1 μM concentration, **P_3AmM** and **TMPyP** resulted in inhibition zones of 1.2 and 1.1 cm, respectively. However, **TMPyPZ** displayed lower antibacterial activity (Photoplate S1, Table S5, and Figure 7A).

Previous studies indicated that lower concentrations of the compounds resulted in weaker associations with bacterial cells, while higher concentrations led to aggregations that prevented

https://doi.org/10.1021/acsomega.4c09535
ACS Omega 2025, 10, 22482−22507

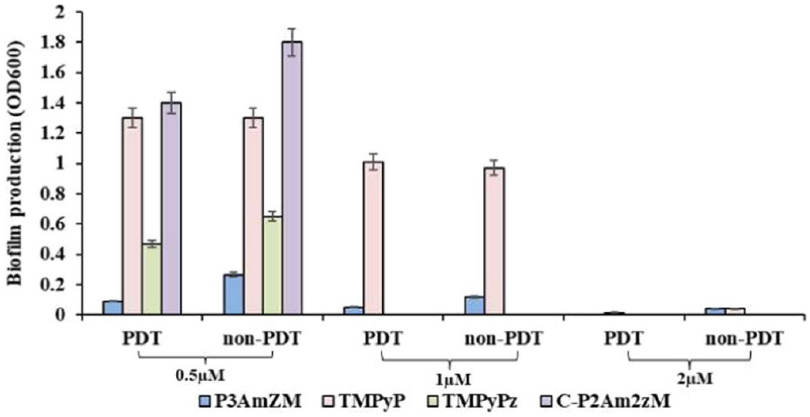

Figure 10. Quantification of biofilm production by *E. coli* in the presence of porphyrin compounds in PDT and non-PDT conditions.

interaction with the bacterial cell wall. Therefore, an optimal moderate concentration was recommended for maximum inhibition of bacterial cells.

The susceptibility of *S. aureus* to the porphyrin compounds was notably higher. Under non-PDT conditions, c-**P_2Am_2M** and **PAm_3ZM** exhibited significant inhibition zones, measuring 3.5 and 3 cm, respectively. Under PDT conditions, c-**P_2Am_2ZM** and **P_3AmZM** showed increased antibacterial activity at 1 μM concentrations, with **P_3AmM** resulting in a 1.2 cm inhibition zone. However, **PAm_3M**, **TMPyP**, and **TMPyPZ** exhibited lower antibacterial activity against *S. aureus* in both PDT and non-PDT conditions. At 2 μM concentrations, antibacterial activity decreased, suggesting that aggregation inhibited compound activity at high concentrations (Photoplate S1, Table S6, and Figure 7B). The findings demonstrate that, under PDT conditions, **P_3AmZM** and c-**P_2Am_2ZM** were the most effective compounds against *E. coli*, and *S. aureus*, followed by **P_3AmM, c-P_2Am_2M, PAm_3ZM, PAm_3M, TMPyP**, and **TMPyPZ**.

Porphyrins exhibit antimicrobial properties to catalyze peroxidase and oxidase reactions, absorb photons, generate reactive oxygen species (ROS), and incorporate into the lipids of bacterial membranes.[26] Batishchev et al.,[78] successfully determined the relationship between the structure and activity of PSs in terms of their antimicrobial properties for two Gram-negative bacteria, *E. coli* and *Acinetobacter baumannii*. Remarkably, with minimal light exposure of 5 J/cm^2, this molecule exhibited inhibition of *E. coli* and *A. baumannii*. This finding positions it as a promising candidate for combating microbial infections. Research has shown that aPDT has proven to be highly effective in eradicating a clinical isolate of *Pseudomonas aeruginosa*, an important pathogen often encountered in healthcare environments.[79] A study conducted by Orenstein et al.[80] demonstrated the efficacy of deuteroporphyrin in eliminating *S. aureus*. Nevertheless, deuteroporphyrin did not exhibit the same inhibitory effect on bacteria such as *E. coli* and *P. aeruginosa*. This issue can be addressed by applying pretreatment to the cells using either ethylenediaminetetraacetic acid (EDTA) or Polymyxin B nonapeptide (PMBN).[81]

2.3.2. Minimal Inhibitory Concentration (MIC) of the Porphyrin Compounds. Control bacterial isolates grew consistently within 24 h. *E. coli* was inhibited at 0.084 mg/mL of **PAm_3ZM** under light conditions, while *S. aureus* required higher concentrations at 0.252 and 0.112 mg/mL in non-PDT and PDT conditions, respectively. MIC values for **P_3AmZM** were 0.97 and 0.388 mg/mL for dark and light conditions, respectively for *E. coli*, and 0.776 and 0.291 mg/mL for *S. aureus*. **c-P_2Am_2ZM** inhibited *S. aureus* at 0.837 and 0.186 mg/mL in non-PDT and PDT conditions, respectively, with MICs of 0.456 and 0.279 mg/mL for *E. coli*. Similarly, **c-P_2Am_2M** inhibited *S. aureus* at 0.88 and 0.22 mg/mL, with MICs of 1.10 and 0.33 mg/mL for *E. coli*. **P_3AmM** showed inhibition at 192 mg/mL in PDT conditions, with higher MICs for *S. aureus* (0.768 mg/mL) compared to *E. coli* (0.480 mg/mL) in dark treatment. **PAm_3M**, **TMPyP**, and **TMPyPZ** exhibited MICs ranging from 0.744 to 0.99 mg/mL in dark conditions and 0.372 to 0.792 mg/mL in the presence of light (Table S7). Agnihotri et al.[82] synthesized citrate-stabilized silver nanoparticles (AgNPs) ranging from 5 to 100 nm, demonstrating antibacterial efficacy against both (*E. coli* MTCC 443 and *S. aureus* NCIM 5201) bacteria. Smaller nanoparticles (5−10 nm) exhibited increased antibacterial efficiency. According to Valduga et al.[83] **TMPyP** efficiently inactivates *E. coli* under visible light by disrupting enzymatic and transport activities of membranes.

2.3.3. Effect of Porphyrins on the Growth Profile and Biofilm Producing Ability of the Bacterial Isolates. Under photodynamic therapy (PDT) conditions, the compounds c-**P_2Am_2ZM** and c-**P_2Am_2M** demonstrated significant bactericidal activity against *E. coli* at concentrations of 0.46 and 0.93 mg/mL, respectively (Figure 8A,B). These treatments resulted in a reduction in bacterial cell population by 98% at 92 h and 100% at 120 h. Similarly, the compounds **P_3AmZM** and **PAm_3M** inhibited bacterial growth at concentrations of 0.97 and 0.93 mg/mL, respectively (Figure 8C,D), achieving a reduction in cell population by 94% at 120 h. Furthermore, **TMPyP** and **TMPyPZ** exhibited a 90% reduction in bacterial growth after a 5-day incubation period at concentrations of 0.99 and 0.98 mg/mL, respectively (Figure 8E,8F). **PAm_3ZM** showed bactericidal activity at 0.28 mg/mL, reducing bacterial growth by 93% at 120 h, whereas **P_3AmM** exhibited a 90% reduction in bacterial growth at 0.96 mg/mL after 96 h (Figure 8G,H).

Compounds c-**P_2Am_2ZM** and c-**P_2Am_2M** completely inhibited *S. aureus* growth (100% reduction) within 5 days at concentrations of 0.93 and 1.10 mg/mL under PDT conditions (Figure 9A,9B). **P_3AmZM** and **PAm_3M** reduced *S. aureus* growth by up to 96% at concentrations >0.49 mg/mL (Figure 9C,9D) at 96 h. **TMPyP** and **TMPyPZ** efficiently killed bacteria at concentrations >0.50 mg/mL (Figure 9E,F), achieving a 92% reduction at 72 h. The growth of *S. aureus* was reduced by up to 96% for **PAm_3ZM** and **P_3AmM** at

https://doi.org/10.1021/acsomega.4c09535
ACS Omega 2025, 10, 22482−22507

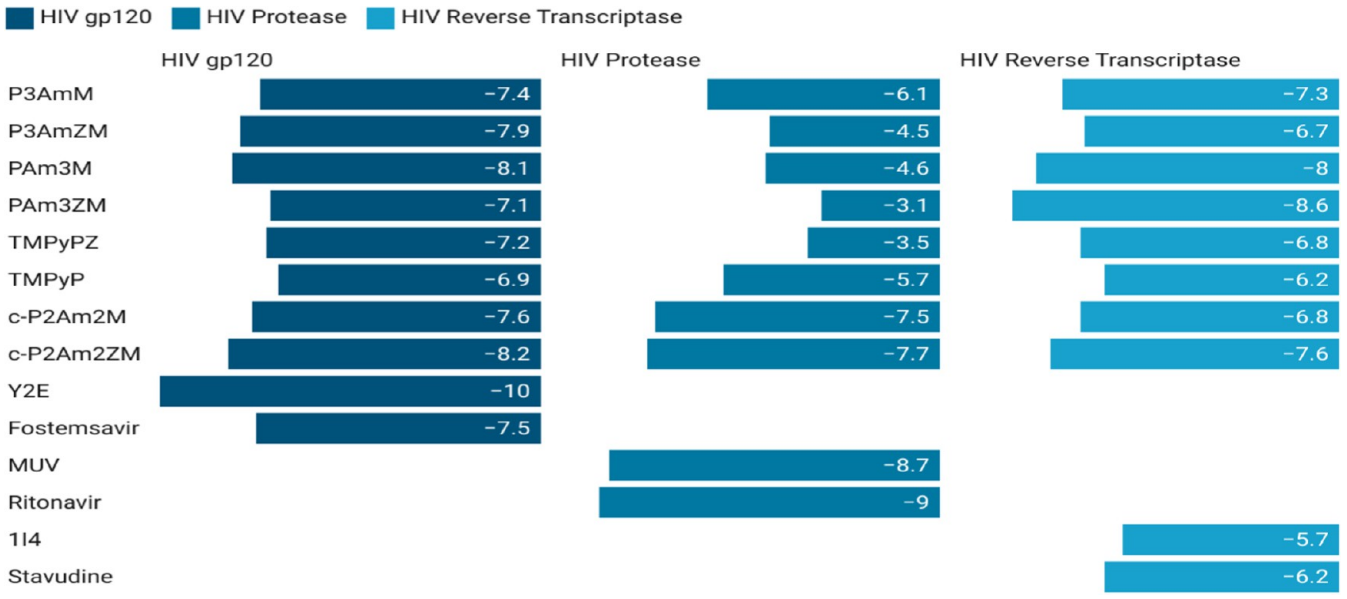

Figure 11. Binding energy details of compounds, drugs, and cocrystallized ligands.

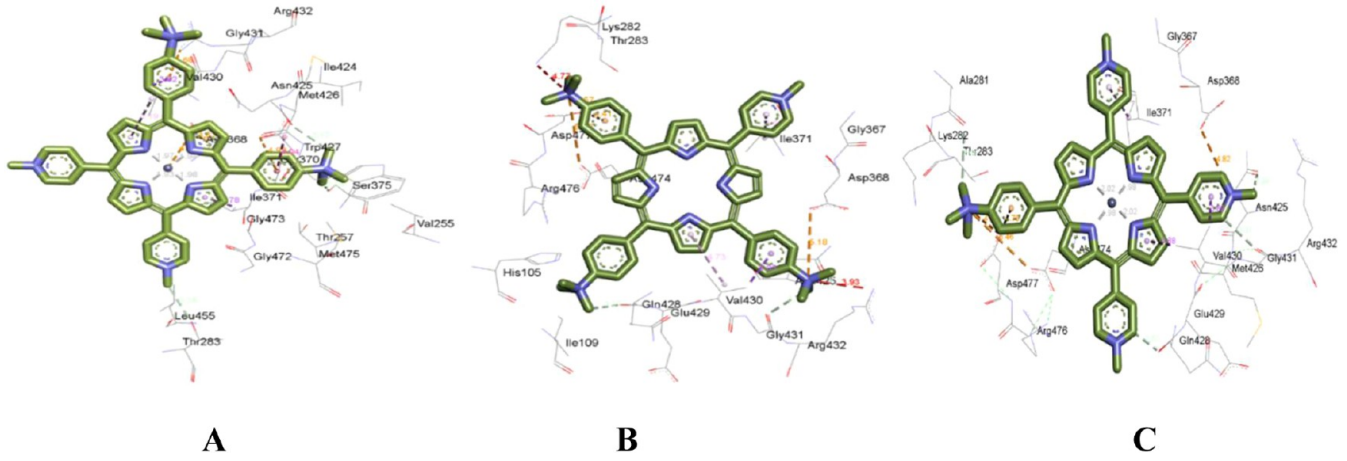

Figure 12. 3D molecular representation of interactions of compounds (A) **c-P_2Am_2ZM**, (B) **P_3AmZM**, and (C) **PAm_3M** with the active site residues of HIV gp120 protein. Interactions were displayed as color-coded dashed lines.

concentrations of 0.97 and 0.93 mg/mL, respectively, at 96 h (Figure 9G,H). Culture samples from each experiment were collected at intervals from 24 to 120 h of incubation and spread onto Nutrient Agar (NA) plates. Colony-forming units (CFU) were counted after incubation at 37 °C for 24 h. The percentage decrease in the cell population was determined. At the killing concentration of the porphyrin compounds, no growth was observed on the agar plates. The results were compared with control groups.

2.3.4. Biofilm Producing Ability of the Bacterial Isolates in the Presence of Porphyrin Compounds. Porphyrin compounds were more effective against *S. aureus* than *E. coli* in both PDT and non-PDT conditions. This study demonstrated that in the presence of c-**P_2Am_2ZM**, **P_3AmZM**, **PAm_3ZM**, **TMPyPZ**, **P_3AmM**, **PAm_3M**, and c-**P_2Am_2ZM**, *S. aureus* exhibited no biofilm formation under both PDT and non-PDT conditions. In non-PDT conditions, *E. coli* formed biofilms at lower concentrations of porphyrin compounds, including **P_3AmZM**, **TMPyP**, **TMPyPZ**, and c-**P_2Am_2ZM**. **P_3AmZM** notably reduced biofilm production in both PDT and non-PDT conditions. At 2 μM concentrations, **TMPyPZ** and c-**P_2Am_2ZM** showed no biofilm formation under both conditions, indicating an inability to produce biofilm even in the presence of growth when exposed to sublethal concentrations of porphyrin-treated samples (Figure 10).

Seeger et al.,[84] examined the antibacterial properties of a zinc(II) metalloporphyrin (ZnTMeP) against biofilms of *Moraxella bovis* and *Moraxella bovoculi*. The compound showed promising results in deactivating *Moraxella* spp. in its planktonic form. Orlandi et al.,[85] tested 13 diaryl-porphyrins for antimicrobial photodynamic therapy (aPDT) and found that dicationic porphyrin (P11) significantly inhibited biofilms without toxicity. This study supports the effectiveness of porphyrins as photoactivated antimicrobials in various clinical and environmental conditions.[86] A dose of 2.5 mg/mL of **TMPyP** tetratosylate achieved maximal toxicity (>99%) against clinical strains of *P. aeruginosa*; higher concentrations (5 mg/mL) were required to inhibit bacteria in biofilms.[87]

2.4. Molecular Docking Outcomes. The docking simulations conducted on HIV target proteins indicate that compounds **c-P_2Am_2ZM**, **PAm_3M**, **P_3AmZM**, **P_3AmM**, **PAm_3ZM**, and **c-P_2Am_2M** demonstrate superior binding

https://doi.org/10.1021/acsomega.4c09535
ACS Omega 2025, 10, 22482−22507

affinity and interaction profiles. Notably, among all the targets examined, these compounds exhibited stronger binding energy with reverse transcriptase compared to gp120 and protease. Specifically, when targeting reverse transcriptase, all compounds displayed better binding energy than stavudine and 1l4 (Figure 11). Furthermore, **c-P_2Am_2ZM** and **c-P_2Am_2M** exhibited superior binding energy with protease compared to other targets. Interestingly, **c-P_2Am_2ZM** emerges as one of the top three compounds across all three explored HIV targets. Additionally, **PAm_3M** stands out as a top compound with gp120 and reverse transcriptase proteins.

In the docking program's validation process, Y2E was meticulously redocked into its cocrystallized site on the HIV gp120 protein. A notably low root mean square deviation (RMSD) value of 1.53 Å was noted between the docked and native poses. This result serves as compelling evidence of the program's ability to accurately predict the binding poses of inhibitors within HIV proteins. This demonstrates the program's capability to reproduce the spatial positioning of Y2E within its designated binding site, affirming the docking algorithm's reliability and precision. The binding energies and molecular interaction profiles of the compounds were compared with those of cocrystallized ligands and drugs targeting various HIV targets. These targets play crucial roles in different stages of the viral life cycle: viral entry (gp120), production of infectious virions (protease), and replication (reverse transcriptase) (Figure 12).

Binding energy and interaction summary of the compounds with HIV proteins.

c-P_2Am_2ZM displayed a distinct binding orientation compared to other top compounds by positioning its trimethyl amino group deeper within the active site pocket. In contrast, the other two compounds were situated on the outer periphery of the gp120 active site pocket. This distinction in positioning can be observed in Figure 13. Both **c-P_2Am_2ZM**, **c-P_2Am_2M**, and **P_3AmM** exhibited a consistent orientation within the protease active site cavity. Tables 3 and 4 presents a detailed overview of the binding energy and molecular interaction profiles of the compounds with HIV gp120 and protease (Figure 14).

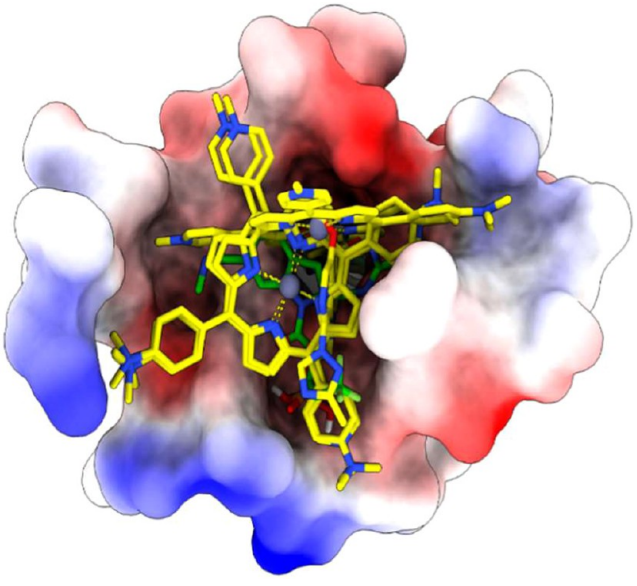

Figure 13. Protein−ligand complexes representing the binding modes of **c-P_2Am_2ZM**, **P_3AmZM**, and **PAm_3M** compounds displayed in yellow color in the active site pocket of HIV gp120.

They projected their trimethyl amino groups deeper into the pocket to establish interactions with crucial active site residues. This observation is illustrated in Figure 15. However, all the top compounds aligned well within the reverse transcriptase active site pocket, as depicted in Figure 17 and their binding energy and interaction profiles are summarized in Table 5.

Across the spectrum of HIV protein targets, including gp120, protease, and RT, the porphyrin analogue **t-P_2Am_2M**, characterized by a trans configuration of groups, consistently demonstrated lower binding energies compared to its cis counterparts. The consistent decrease in binding efficacy observed with the trans arrangement emphasizes the critical role of the spatial orientation of molecular groups within the porphyrin structure in effectively targeting HIV protein sites.

For details regarding the binding energy and corresponding molecular interactions of **t-P_2Am_2M**, please refer to the Supporting Information (Table S9 and Figure S4).

3. DISCUSSION

In the present study, we have established the potential of newly synthesized ammonium phenyl porphyrins to inhibit HIV infection. There is no evidence of any similar investigation being performed previously on these porphyrins. These porphyrins exerted antiviral activity in the lower nanomolar range under PDT conditions without any evident cytotoxicity. Under PDT conditions, they completely blocked virus entry inside the target cells as well as the HIV-1 production in infected cells. The antiviral activity was not affected by zinc metalation or by the presence of different combinations of ammonium phenyl or pyridinium groups. Our results suggested ammonium phenyl porphyrins may act as active photosensitizers against HIV-1 blocking both virus entry as well as virus production in infected cells. The plausible mechanism could be their ability to absorb photons as photosensitizers generating ROS that confers photodynamic inactivation of HIV-1. Porphyrins targeting HIV-1 entry as well as production may serve as one of the promising antiviral therapeutics.

On the contrary, under non-PDT conditions, ammonium phenyl porphyrins were not toxic up to the range of concentration tested (10 μM). However, porphyrins failed to inhibit HIV-1 entry significantly. However, virus production was modestly affected depending upon the zinc metalation, and the number of ammonium phenyl and pyridinium groups present. In addition, the infectivity of HIV-1 produced in the presence of ammonium phenyl porphyrin was significantly reduced. These results demonstrated antiviral activity of ammonium phenyl porphyrins was enhanced upon exposure to light. Hence ammonium phenyl porphyrins emerge as active photosensitizers against HIV-1.

Another significant finding of this study is the superior effectiveness of porphyrin compounds against *S. aureus* compared to *E. coli* under both photodynamic therapy (PDT) and non-PDT conditions. Porphyrins, used as photosensitizing molecules, present a robust approach for the elimination of microorganisms and biofilms via photodynamic therapy. Under both conditions, *S. aureus* exhibited no biofilm formation in the presence of compounds such as **c-P_2Am_2ZM**, **P_3AmZM**, **PAm_3ZM**, **TMPyPZ**, **P_3AmM**, and **PAm_3M**. Conversely, *E. coli* formed biofilms at lower concentrations of porphyrin compounds, including **P_3AmZM**, **TMPyP**,

https://doi.org/10.1021/acsomega.4c09535
ACS Omega 2025, 10, 22482−22507

Table 3. Molecular Interaction Summary of Top Compounds with HIV gp120

compounds	binding energy (K cal/mol)	interacting amino acids	nature of interactions
c-P_2Am_2ZM	−8.2	ILE371, MET426, GLU370, ASP368, ARG432, VAL430, SER375, ASN425, THR283	Amide−π stacked, π−sigma, π−alkyl, π−cation, π−anion, carbon−hydrogen bond, van der Waals
PAm_3M	−8.1	ILE371, GLY473, ASP477, ASP474, GLN428, VAL430, ASP368, GLY431, ASN425	Amide−π stacked, π−sigma, π−alkyl, π−anion, π−anion, carbon−hydrogen bond, van der Waals
P_3AmZM	−7.9	ILE371, ASP474, ASP477, ALA281, GLY473, GLN428, GLY431, VAL430, ASN425, ASP368	Amide−π stacked, π−sigma, π−alkyl, π−anion, π−anion, carbon−hydrogen bond, van der Waals

Table 4. Molecular Interaction Summary of Top Compounds with HIV Protease

compounds	binding energy (K cal/mol)	interacting amino acids	nature of interactions
c-P_2Am_2ZM	−7.7	ASP25, LEU23, ARG8, VAL82, PRO81	π−cation, π−alkyl, carbon−hydrogen bond, van der Waals
c-P_2Am_2M	−7.5	ASP25, LEU23, ARG8, VAL82, PRO81	π−π-cation, π−alkyl, carbon−hydrogen bond, van der Waals
P_3AmM	−6.1	ASP30, ASP29, ALA28, ARG8, VAL82, LEU23	π−anion, π−cation, π−sigma, π−alkyl, carbon−hydrogen bond, van der Waals

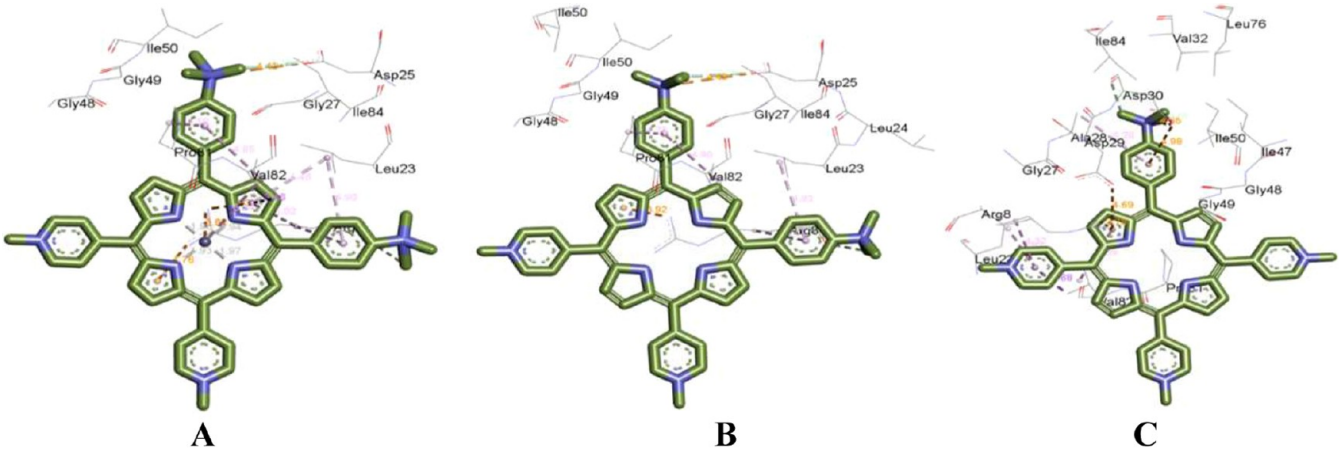

Figure 14. 3D molecular representation of interactions of compounds (A) **c-P_2Am_2ZM**, (B) **c-P_2Am_2ZM**, and (C) **P_3AmM** with the active site residues of HIV protease. Interactions were displayed as color-coded dashed lines.

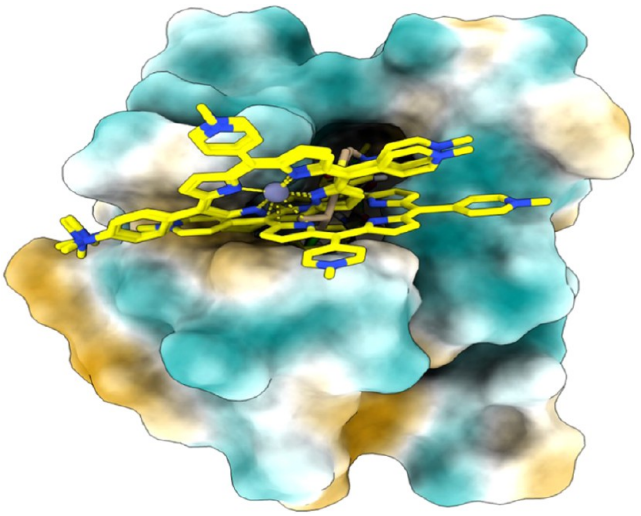

Figure 15. Protein−ligand complexes representing the binding modes of **c-P_2Am_2ZM**, **c-P_2Am_2ZM**, and **P_3AmM** compounds displayed in yellow color in the active site pocket of HIV protease.

TMPyPZ, and **c-P_2Am_2ZM**, in non-PDT conditions. Notably, **P_3AmZM** significantly reduced biofilm production under both PDT and non-PDT conditions. Furthermore, **TMPyPZ** and **c-P_2Am_2ZM**, at concentrations of 2 μM, completely inhibited biofilm formation in both conditions, indicating their capability to prevent biofilm formation even when exposed to sublethal concentrations of porphyrin-treated samples. In conclusion, this study highlights the potential of porphyrin compounds as effective antimicrobial agents against both planktonic and biofilm forms of bacterial pathogens. Their demonstrated efficacy under PDT conditions emphasizes the importance of advancing photodynamic therapy as a viable treatment strategy for combating bacterial infections and preventing biofilm-associated complications. However, further research is required to determine the interaction between these compounds and bacterial cells, which will be crucial for understanding their mechanism of action. Recent studies have demonstrated the significant potential of porphyrin compounds and photodynamic therapy (PDT) in combating bacterial pathogens, including those forming biofilms and exhibiting antibiotic resistance. Anas et al.,[88] showed the mechanisms by which PDT, using porphyrin photosensitizers, generates reactive oxygen species to induce microbial cell death, highlighting its broad-spectrum efficacy. Liu et al.,[89] further emphasized the promise of antimicrobial PDT (aPDT) in eradicating antibiotic-resistant bacteria and biofilms. Fu et al.,[90] showed differential efficacy of porphyrin compounds against MRSA, attributed to their cell wall structures. Karygianni et al.,[91] reviewed the success of aPDT in disrupting biofilms. Dharmaratne et al.[92] provided in vivo evidence of PDT's

https://doi.org/10.1021/acsomega.4c09535
ACS Omega 2025, 10, 22482−22507

Table 5. Molecular Interaction Summary of Top Compounds with HIV Reverse Transcriptase

compounds	binding energy (K cal/mol)	interacting amino acids	nature of interactions
PAm_3ZM	−8.6	ARG72, LYS66, LEU74, TYR115, MET184, ALA114, ASP185, PHE160	$\pi-\pi$ T-shaped, π−alkyl, π−cation, π-sigma, carbon−hydrogen bond, van der Waals
PAm_3M	−8.0	ARG72, LYS66, LEU74, GLY152, MET184, ALA114, ASP185, TYR115	$\pi-\pi$ T-shaped, π−alkyl, π−cation, π−sigma, carbon−hydrogen bond, van der Waals
c-P_2Am_2ZM	−7.6	ARG72, LYS66, LEU74, ASP185, TYR115, MET184, ALA114	$\pi-\pi$ T-shaped, π−alkyl, π−cation, π−sigma, carbon−hydrogen bond, van der Waals

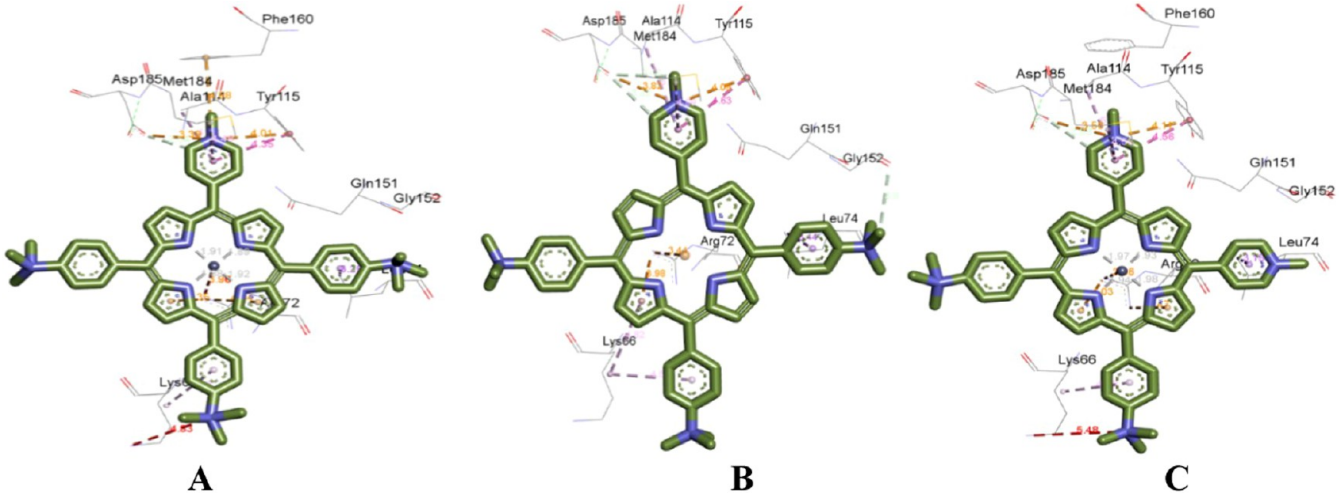

Figure 16. 3D molecular representation of interactions of compounds (A) **PAm_3ZM**, (B) **PAm_3M**, and (C) **c-P_2Am_2ZM** with the active site residues of HIV reverse transcriptase. Interactions were displayed as color-coded dashed lines.

effectiveness in reducing *S. aureus* biofilm viability. Collectively, these studies underscore the robust antimicrobial activity of porphyrins under PDT, advocating for its development as a viable treatment modality against infections, particularly those involving resistant strains and biofilms.

4. CONCLUSIONS

Six hydrophilic cationic porphyrins (CPs), namely **P_3AmM**, **c-P_2Am_2M**, **PAm_3M**, **P_3AmZM**, **c-P_2Am_2ZM**, and **PAm_3ZM**, were synthesized through rigorous methylation of precursor free-base aminophenyl porphyrins and their zinc complexes. This involved quaternarization of *meso*-(4-aminophenyl) to *meso*-(4-trimethylammonium phenyl) groups and simultaneous alkylation of *meso*-(4-pyridyl) to *meso*-(4-methylpyridinium) moieties using methyl iodide under reflux conditions. Upon investigation, these ammonium phenyl porphyrins demonstrated minimal entry inhibitory effects on HIV-1 in the non-PDT, yet exhibited significant inhibition upon photoirradiation, with varying degrees of effectiveness. None of the compounds showed toxicity under test conditions. Moreover, the CPs effectively reduced HIV-1 infectivity, both in terms of entry and production, with **c-P_2Am_2M** and **c-P_2Am_2ZM** showing particularly promising results. The demonstrated effectiveness of the compounds in inhibiting HIV entry (gp120), production (reverse transcriptase), and infectivity (protease) aligns closely with their enhanced binding affinity and interaction profiles (Figures 12, 14, and 16) revealed in docking simulations against the pertinent HIV targets responsible for these functions. With positive outcomes observed in both in vitro studies and molecular docking evaluations, these compounds deserve further investigation as prospective candidates in the quest for anti-HIV agents The study suggests a structure−activity relationship, indicating that an equitable presence of *meso*-ammonium phenyl and *meso*-pyridinium groups contributes to enhanced photobiological activity. In contrast, a decrease in *meso*-pyridinium groups correlates with reduced activity of the porphyrins. These findings underscore the potential of these compounds as antidrug-resistant antibiotics and as anti-HIV agents. Further, the antimicrobial activity of the porphyrin compounds showed that **P_3AmZM** and **c-P_2Am_2ZM** were highly effective against bacterial pathogens. Moreover, the compounds also showed antibiofilm activity and inhibition of bacterial growth within a five-day period of time. The MIC results showed **PAm_3ZM** is highly effective against *E. coli* under light conditions. Under PDT conditions, all compounds demonstrated significant bactericidal activity against *E. coli* and *S. aureus*. Exposure to light enhanced the antibacterial activity of all compounds, where lower MIC values were recorded as compared to dark conditions. **c-P_2Am_2ZM** and **c-P_2Am_2M** showed the highest efficacy, completely inhibiting bacterial growth. These findings confirm the antibacterial and antiviral activities of **c-P_2Am_2ZM** and **c-P_2Am_2M** compounds, with prospects of their potential use in controlling such infections (Figures 15 and 17).

5. EXPERIMENTAL SECTION

5.1. Synthesis. Pyridine-4-carboxaldehyde, iodoacetic acid, C_{60}, zinc acetate dihydrate (Sigma-Aldrich), 4-acetamidobenzaldehyde, and propionic acid (Merck), were used without further purification. Pyrrole (Sigma-Aldrich) was freshly distilled before use. $CHCl_3$ (HPLC grade), and MeOH (HPLC grade) (Sigma-Aldrich) were used as received. All other solvents used were purified using standard purification and drying techniques. Silica gel (60−200 mesh, and 100−200 mesh, SRL) was employed for column chromatography.

https://doi.org/10.1021/acsomega.4c09535
ACS Omega 2025, 10, 22482−22507

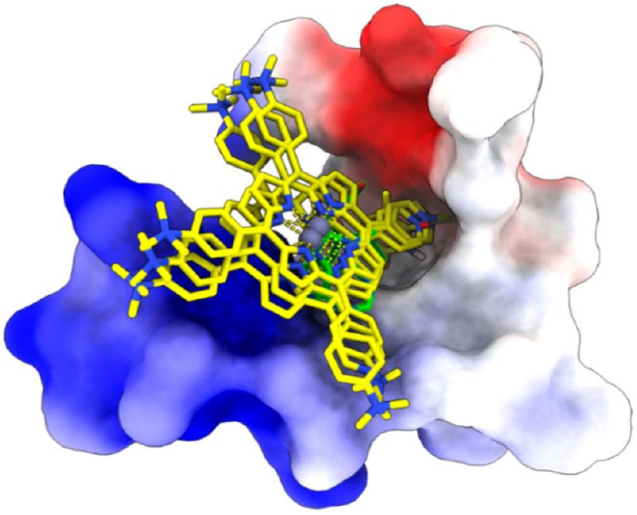

Figure 17. Protein−ligand complexes representing the binding modes of **c-P_2Am_2ZM**, **P_3AmZM**, and **PAm_3M** compounds displayed in yellow color in the active site pocket of HIV reverse transcriptase.

UV−visible absorption spectra were recorded using a Jasco V-730 spectrophotometer in the range 200 to 800 nm (steps of 0.5 nm) in a 1 mm quartz cuvette using either dimethylformamide (DMF) or water as the solvent at a temperature of 298 K, the spectral bandpass being 1 nm. The emission spectra were recorded using a Fluoromax-4 spectrofluorometer (Horiba Scientific), at 298 K, in a 1 mm quartz cuvette, the solvent used for data acquisition was either DMF or water. The slit widths for both the excitation and emission monochromators were set at 5 nm. In a typical experiment fixed-concentration solutions of the compounds were excited at the absorption maxima (λ_{max}) of their respective Soret Band absorptions. ^{1}H NMR data were recorded with a Bruker Av III HD 400 MHz spectrometer or a Bruker Avance III 400 MHz spectrometer in $CDCl_3$ or DMSO-d6 with TMS as an internal standard. MALDI-TOF spectra were recorded with AB Sciex 4000 Q-Trap-Mass Spectrometer or a Bruker Autoflex max LRF mass spectrometer.

5.1.1. Synthesis and Isolation of 5-(4-Acetamidophenyl)-10,15,20-tri-(4-pyridyl) Porphyrin (P_3A). A 500 mL RB flask, equipped with a magnetic stir bar, condenser, and a silica gel guard tube, was charged with propionic acid (180 mL) and subjected to heating for 10 min at 110 °C. After that, 4-acetamidobenzaldehyde (3.52 g, 0.021 mol, 1.5 equiv) and pyridine-4-carboxaldehyde (4.33 mL, 0.045 mol, 3.2 equiv) were added to it, followed by the addition of pyrrole (4 mL, 0.057 mol, 4 equiv), dropwise, for 20 min. The reaction mixture was protected from light. After stirring at 150 °C for 90 min, the excess propionic acid was entirely removed by distillation. Neutralization of the crude product was achieved by using 0.5 M ammonia solution, and the residue collected by filtration was washed with copious amounts of water, followed by cold diethyl ether. The dark impurified product was loaded in a silica gel column and eluted with 0.5% Et_3N in 3−5% methanol in dichloromethane as the eluent. The porphyrin fractions were concentrated and then separated on a second silica gel column with 5% methanol in dichloromethane to yield 999 mg (10.2%) of the target compound **P_3A**.

5.1.1.1. P_3A. UV−vis (DMF at 1 μM concentration), 645 nm (λ_{max}, Q-band), 590 nm (λ_{max}, Q-band), 548 nm (λ_{max}, Q-band), 513 nm (λ_{max}, Q-band), 418 nm (λ_{max}, Soret band). Emission (DMF at 1 μM concentration) (λ_{ex}.= 418 nm, S-band): 644, 660 nm Q(0,0), 717 nm Q(0,1); with Stokes shift 242 nm Q(0,0)-B(0,0). ^{1}H NMR (400 MHz, DMSO-d_6, 298 K) δ = 9.05 (d, J = 4.1 Hz, 6H), 8.94 (d, J = 4.7 Hz, 2H, β-pyrrole), 8.85 (s, 4H), 8.82 (d, J = 4.7 Hz, 2H, β-pyrrole), 8.18 (s, 1H), 8.16 (d, J = 4.1 Hz, 6H), 7.94 (d, J = 7.9 Hz, 2H), 7.56 (d, J = 7.9 Hz, 2H), 2.38 (s, 3H), −2.84 (s, 2H). HRMS (ESI) Calcd for $C_{43}H_{30}N_8O$ $[M + H]^+$ m/z 675.2621, found 675.2638.

The one-pot synthesis resulted in the formation of **5,10-di(4-acetamidophenyl)-15,20-di(4-pyridyl) porphyrin (c-P_2A_2)** and **5,10,15-tri-(4-acetamidophenyl)-20-(4-pyridyl) porphyrin (PA_3)** as well. **c-P_2A_2** (Yield: 950 mg, 9%) and **PA_3** (Yield: 750 mg, 6%) eluted out with 5% MeOH in DCM and 7% MeOH in DCM respectively. All the compounds were characterized using a combination of spectroscopic techniques.

5.1.1.2. c-P_2A_2. UV−vis (DMF at 1 μM concentration), 648 nm (λ_{max}, Q-band), 591 nm (λ_{max}, Q-band), 551 nm (λ_{max}, Q-band), 515 nm (λ_{max}, Q-band), 420 nm (λ_{max}, Soret band). Emission (DMF at 1 μM concentration) (λ_{ex}.= 420 nm, S-band): 647, 664 nm Q(0,0), 720 nm Q(0,1); with Stokes shift 244 nm Q(0,0)-B(0,0). ^{1}H NMR(400 MHz, $CDCl_3$, 100.15 K) δ = 9.05 (d, J = 5 Hz, 4H), 8.92 (d, J = 4.7 Hz, 2H, β-pyrrole), 8.89 (s, 2H, β-pyrrole), 8.83 (s, 2H, β-pyrrole), 8.8 (d, J = 4.7 Hz, 2H, β-pyrrole), 8.17 (s, 2H), 8.16 (d, J = 4.1 Hz, 4H), 7.92 (d, J = 7.9 Hz, 4H), 7.53 (d, J = 7.9 Hz, 4H), 2.38 (s, 6H), −2.84 (s, 2H). HRMS (ESI) Calcd for $C_{46}H_{34}N_8O_2$ $[M + H]^+$ m/z 731.2883, found 731.2908.

5.1.1.3. PA_3. UV−vis (DMF at 1 μM concentration), 649 nm (λ_{max}, Q-band), 592 nm (λ_{max}, Q-band), 553 nm (λ_{max}, Q-band), 516 nm (λ_{max}, Q-band), 422 nm (λ_{max}, Soret band). Emission (DMF at 1 μM concentration) (λ_{ex}.= 422 nm, S-band): 646, 673 nm Q(0,0), 723 nm Q(0,1); with Stokes shift 251 nm Q(0,0)-B(0,0). ^{1}H NMR (400 MHz, DMSO-d_6, 298 K) δ = 10.41 (s, 3H), 9.04 (d, J = 4.9 Hz, 2H), 8.92 (d, J = 4.2 Hz, 2H, β-pyrrole), 8.89 (s, 4H, β-pyrrole), 8.84 (d, J = 4.2 Hz, 2H, β-pyrrole), 8.27 (d, J = 4.9 Hz, 2H), 8.15 (d, J = 8.1 Hz, 6H), 8.06 (d, J = 8.1 Hz, 6H), 2.24 (s, 9H), −2.92 (s, 2H). HRMS (ESI) Calcd for $C_{49}H_{38}N_8O_3$ $[M + H]^+$ m/z 787.3145, found 788.3223.

5.1.2. Synthesis and Isolation of 5-(4-Aminophenyl)-5,10,15-tri-(4-pyridyl) Porphyrin (P_3Am). Compound **P_3A** (250 mg, 0.370 mmol) was dissolved in ethanol (20 mL) in a 150 mL single-neck RB flask fitted with a reflux condenser and silica gel guard tube. After that, 5 M HCl (100 mL) was added to the flask, and the contents were set to reflux. Reflux was continued for 3 h, at the end of which 200 mL water was added to the reaction mixture, and the pH was adjusted to 7 using a 5 M NH_3 solution. The product obtained was extracted through solvent extraction with dichloromethane and water. The organic layer was collected over Na_2SO_4 and kept standing for 4 h. After that, the solvent was collected by filtration, and the filtrate was concentrated on a rotary evaporator. The rotary concentrate was dissolved in a minimum volume of DCM, and the pure product precipitated from it by gradually adding hexane. Color: Purple, Yield: 206 mg (88%).

P_3Am UV−vis: (DMF, 1 μM Solution), 650 nm (λ_{max}, Q-band), 590 nm (λ_{max}, Q-band), 557 nm (λ_{max}, Q-band), 515 nm (λ_{max}, Q-band), 416 nm (λ_{max}, Soret band). Emission (DMF at 1 μM concentration) (λ_{ex} = 416 nm, S-band), 653 nm Q(0,0), 718 nm Q(0,1), with Stokes shift 237 nm Q(0,0)-B(0,0). ^{1}H NMR (400 MHz, $CDCl_3$, 100.15 K) δ = 9.05 (d, J = 4.7 Hz, 6H), 9.02 (d, J = 5 Hz, 2H, β-pyrrole), 8.84 (s, 4H,

https://doi.org/10.1021/acsomega.4c09535
ACS Omega 2025, 10, 22482−22507

β-pyrrole), 8.83 (d, J = 5 Hz, 2H, β-pyrrole), 8.16 (d, J = 4.7 Hz, 6H), 7.99 (d, J = 8.2 Hz, 2H), 7.09 (d, J = 8.2 Hz, 2H), −2.84 (s, 2H). HRMS (ESI) Calcd for $C_{49}H_{38}N_8O_3$ $[M + H]^+$ m/z 633.2515, found 633.2533.

Similar procedures were employed to synthesize **5,10-di(4-aminophenyl)-15,20-di(4-pyridyl) porphyrin (c-P_2Am_2)** and **5,10,15-tri-(4-aminophenyl)- 20-(4-pyridyl) porphyrin (PAm_3)** with yields of 96 and 82%.

5.1.2.1. c-P_2Am_2. UV−vis: (DMF, 1 μM Solution), 656 nm (λ_{max}, Q-band), 596 nm (λ_{max}, Q-band), 564 nm (λ_{max}, Q-band), 519 nm (λ_{max}, Q-band), 422 nm (λ_{max}, Soret band). Emission (DMF at 1 μM concentration) (λ_{ex} = 422 nm, S-band), 673 nm Q(0,0), 723 nm Q(0,1), with Stokes shift 251 nm Q(0,0)-B(0,0). ^{1}H NMR (400 MHz, $CDCl_3$, 100.15 K) δ = 9.03 (d, J = 5.6 Hz, 4H), 8.99 (d, J = 5 Hz, 2H, β-pyrrole), 8.95 (s, 2H, β-pyrrole) 8.81 (s, 2H, β-pyrrole), 8.77 (d, J = 5 Hz, 2H, β-pyrrole), 8.16 (d, J = 5.6 Hz, 4H), 7.99 (d, J = 8.5 Hz, 4H), 7.08 (d, J = 8.2 Hz, 4H), 4.45 (s, br, 1H), 4.06 (s, br, 3H), −2.78 (s, 2H). HRMS (ESI) Calcd for $C_{42}H_{30}N_8$ $[M + H]^+$ m/z 647.2671, found 647.2692.

5.1.2.2. PAm_3. UV−vis: (DMF, 1 μM Solution), 734 nm (λ_{max}, Q-band), 662 nm (λ_{max}, Q-band), 571 nm (λ_{max}, Q-band), 523 nm (λ_{max}, Q-band), 431 nm (λ_{max}, Soret band). Emission (DMF at 1 μM concentration) (λ_{ex} = 431 nm, S-band), 694 nm Q(0,0), 757 nm Q(0,1), with Stokes shift 263 nm Q(0,0)-B(0,0). ^{1}H NMR (400 MHz, $CDCl_3$, 100.15 K) δ = 9.01 (d, J = 4.4 Hz, 2H), 8.95 (d, J = 4.4 Hz, 2H, β-pyrrole), 8.92 (s, 4H, β-pyrrole), 8.75 (d, J = 4.4 Hz, 2H, β-pyrrole), 8.16 (d, J = 4.4 Hz, 2H), 7.99 (d, J = 7.97 Hz, 6H), 7.05 (d, J = 7.3 Hz, 6H), −2.74 (s, 2H). HRMS (ESI) Calcd for $C_{43}H_{32}N_8$ $[M + H]^+$ m/z 661.2828, found 661.2830.

5.1.3. Synthesis and Isolation of 5-(4-Aminophenyl)-5,10,15-tri-(4-pyridyl)−21H,23H−Zn(II) Porphyrin (P_3AmZ). Compound **P_3Am** (0.100 g, 0.158 mmol, 1 equiv) was dissolved in $CHCl_3$ (9 mL) and taken in a stoppered 25 mL RB flask. The flask was charged with a saturated solution of zinc acetate dihydrate in methanol (1 mL), and the contents were left to stir. UV−vis recorded from time to time indicated the completion of the reaction after 12 h. The product formed was recovered by solvent extraction with DCM and water. Upon the accomplishment of the traditional workup, the compound **P_3AmZ** obtained was collected by filtration and dried. Yield: 96 mg, 87%.

5.1.3.1. P_3AmZ. UV−vis: (DMF, 1 μM Solution), 603 nm (λ_{max}, Q-band), 560 nm (λ_{max}, Q-band), 427 nm (λ_{max}, Soret band). Emission (DMF at 1 μM concentration) (λ_{ex} = 427 nm, S-band), 622 nm Q(0,0), 662 nm Q(0,1), with Stokes shift 195 nm Q(0,0)-B(0,0). ^{1}H NMR (400 MHz, DMSO-d_6, 298 K) δ = 9.01 (d, J = 4.6 Hz, 6H), 8.98 (d, J = 4.4 Hz, 2H, β-pyrrole), 8.81 (s, 4H, β-pyrrole), 8.79 (d, J = 4.4 Hz, 2H, β-pyrrole), 8.21 (d, J = 4.6 Hz, 6H), 7.83 (d, J = 8.1 Hz, 2H), 6.99 (d, J = 8.1 Hz, 2H), 5.53 (s, br, 2H). MALDI-TOF Calcd for $C_{41}H_{26}N_8Zn$ $[M]^+$ m/z 694.1572, found 694.315.

Zn-metalation of compounds **c-P_2Am_2** and **PAm_3** was similarly carried out by reaction with zinc acetate dihydrate in $CHCl_3$/MeOH media. **c-P_2Am_2Z** and **PAm_3Z** were obtained in 86 and 78% yield, respectively.

5.1.3.2. c-P_2Am_2Z. UV−vis: (DMF, 1 μM Solution), 607 nm (λ_{max}, Q-band), 563 nm (λ_{max}, Q-band), 432 nm (λ_{max}, Soret band). Emission (DMF at 1 μM concentration) (λ_{ex} = 432 nm, S-band), 634 nm Q(0,0), 678 nm Q(0,1), with Stokes shift 202 nm Q(0,0)-B(0,0). ^{1}H NMR (400 MHz, DMSO-d_6, 298 K) δ = 8.98 (d, J = 4.9 Hz, 4H), 8.94 (d, J = 4.4 Hz, 2H, β-pyrrole), 8.91 (s, 2H, β-pyrrole), 8.77 (s, 2H, β-pyrrole), 8.74 (d, J = 4.4 Hz, 2H, β-pyrrole), 8.19 (d, J = 4.9 Hz, 4H), 7.83 (d, J = 8.1 Hz, 4H), 6.99 (d, J = 8.1 Hz, 4H), 5.55 (s, 4H). MALDI-TOF Calcd for $C_{42}H_{28}N_8Zn$ $[M + H]^+$ m/z 709.1806, found 709.378.

5.1.3.3. PAm_3Z. UV−vis: (DMF, 1 μM Solution), 611 nm (λ_{max}, Q-band), 566 nm (λ_{max}, Q-band), 435 nm (λ_{max}, Soret band). Emission (DMF at 1 μM concentration) (λ_{ex} = 435 nm, S-band), 643 nm Q(0,0), 686 nm Q(0,1), with Stokes shift 208 nm Q(0,0)-B(0,0). ^{1}H NMR (400 MHz, DMSO-d_6, 298 K) δ = 8.97 (d, J = 4.9 Hz, 2H), 8.9 (d, J = 4.6 Hz, 2H, β-pyrrole), 8.88 (s, 4H, β-pyrrole), 8.71 (d, J = 4.6 Hz, 2H, β-pyrrole), 8.19 (d, J = 4.9 Hz, 2H), 7.82 (d, J = 7.8 Hz, 6H), 6.98 (d, J = 7.8 Hz, 6H), 5.48 (s, 6H). MALDI-TOF Calcd for $C_{43}H_{30}N_8Zn$ $[M + H]^+$ m/z, 722.1885, found 722.197.

5.1.4. Synthesis of 5-(4-Trimethylammonium phenyl)-5,10,15-tri-(4-methylpyridinium) Porphyrin (P_3AmM). **P_3Am** (0.05 g, 0.079 mmol, 1 equiv) was taken in a stoppered 10 mL amber-colored RB flask equipped with a magnetic stir bar. The flask was then charged with methyl iodide (5 mL), and the reaction set was then set to stir at 50 °C. TLC indicated the complete consumption of the starting material after 72 h. Excess methyl iodide was removed, and the residue repeatedly washed with diethyl ether and hexane before being dried. Yield: 0.092 g, 92%.

5.1.4.1. P_3AmM. UV−vis: (Water, 10 μM Solution), 641 nm (λ_{max}, Q-band), 583 nm (λ_{max}, Q-band), 558 nm (λ_{max}, Q-band), 518 nm (λ_{max}, Q-band), 421 nm (λ_{max}, Soret band). Emission (Water at 10 μM concentration) (λ_{ex} = 421 nm, S-band), 710 nm, with Stokes shift 289 nm Q(0,0)-B(0,0). MALDI-TOF Calcd for $C_{47}H_{44}N_8I_4$ $[M - 4I]^+$ m/z, 720.3667 found 720.370.

c-P_2Am_2M, **PAm_3M**, **P_3AmZM**, **c-P_2Am_2ZM**, and **PAm_3ZM** were prepared by employing similar reaction condition from **c-P_2Am_2**, **PAm_3**, **P_3AmZ**, **c-P_2Am_2Z**, and **PAm_3Z**.

5.1.4.2. c-P_2Am_2M. UV−vis: (Water, 10 μM Solution), 651 nm (λ_{max}, Q-band), 580 nm (λ_{max}, Q-band), 564 nm (λ_{max}, Q-band), 516 nm (λ_{max}, Q-band), 421 nm (λ_{max}, Soret band). Emission (Water at 10 μM concentration) (λ_{ex} = 421 nm, S-band), 658 nm Q(0,0), 707 nm Q(0,1), with Stokes shift 237 nm Q(0,0)-B (0,0). MALDI-TOF Calcd for $C_{50}H_{50}N_8I_4$ $[M - 4I]^+$ m/z, 762.4136, found 762.416.

5.1.4.3. PAm_3M. UV−vis: (Water, 10 μM Solution), 657 nm (λ_{max}, Q-band), 600 nm (λ_{max}, Q-band), 562 nm (λ_{max}, Q-band), 520 nm (λ_{max}, Q-band), 427 nm (λ_{max}, Soret band). Emission (Water at 10 μM concentration) (λ_{ex} = 427 nm, S-band), 627 nm, with Stokes shift 200 nm Q(0,0)-B(0,0). MALDI-TOF Calcd for $C_{53}H_{56}N_8I_4$ $[M - 4I]^+$ m/z, 804.4606 found 804.464.

5.1.4.4. P_3AmZM. UV−vis: (Water, 10 μM Solution), 605 nm (λ_{max}, Q-band), 561 nm (λ_{max}, Q-band), 432 nm (λ_{max}, Soret band). Emission (Water at 10 μM concentration) (λ_{ex} = 432 nm, S-band), 630 nm Q(0,0), 653 nm Q(0,1), with Stokes shift 198 nm Q(0,0)-B (0,0). MALDI-TOF Calcd for $C_{50}H_{50}N_8I_4$ $[M - 4I]^+$ m/z, 782.2808, found 782.283.

5.1.4.5. c-P_2Am_2ZM. UV−vis: (Water, 10 μM Solution), 604 nm (λ_{max}, Q-band), 560 nm (λ_{max}, Q-band), 428 nm (λ_{max}, Soret band). Emission (Water at 10 μM concentration) (λ_{ex} = 428 nm, S-band), 634 nm Q(0,0), 654 nm Q(0,1), with Stokes shift 206 nm Q(0,0)-B (0,0). MALDI-TOF Calcd for $C_{50}H_{50}N_8I_4$ $[M - 4I]^+$ m/z, 824.3277, found 824.331.

5.1.4.6. PAm_3ZM. UV−vis: (Water, 10 μM Solution), 601 nm (λ_{max}, Q-band), 557 nm (λ_{max}, Q-band), 423 nm (λ_{max},

https://doi.org/10.1021/acsomega.4c09535
ACS Omega 2025, 10, 22482−22507

Soret band). Emission (Water at 10 μM concentration) (λ_{ex} = 423 nm, S-band), 657 nm, with Stokes shift 208 nm Q(0,0)-B(0,0). MALDI-TOF Calcd for $C_{50}H_{50}N_8I_4$ $[M - 4I]^+$ m/z, 804.4606, found 804.464.

5.2. Anti-HIV Studies. *5.2.1. Plasmids and Cell Culture.* HIV-1 subtype B molecular clone NL4−3 was obtained as a kind gift from Dr. Eric O. Freed (National Cancer Institute, NIH). Plasmid DNA was extracted and purified using a Thermo Fisher Scientific Plasmid Maxi Kit as per the manufacturer's directions. All the cell lines were obtained from NIH-HRP program. TZM-bl cells were maintained in Dulbecco's modified Eagle's medium (DMEM) containing 10% fetal bovine serum (FBS). TZM-bl is a HeLa cell line derivative that stably expresses CD4 and CCR5 and thus is highly sensitive to HIV infection. It contains separate copies of luciferase and β-galactosidase genes under the control of the HIV-1 LTR promoter. HIV infection can be quantitatively measured as a function of luciferase or β-galactosidase activity

5.2.2. Preparation of Porphyrin Solution. All the porphyrins were dissolved in a 5% DMSO in water solution (−) used as the control in our experiments. The solution of Enfuvirtide (T20) (positive control) was prepared in DMSO. The antiviral activity of porphyrins was studied in both dark (nonphotodynamic, non-PDT) conditions and Light under specific conditions (Photodynamic conditions, PDT).

5.2.3. Cytotoxicity Assay. Cytotoxicity assay was performed using the Cell Titer-Blue Cell Viability Assay kit (Promega catalogue number: G8080) as per the manufacturer's recommendations. Cells were treated and maintained in the presence or absence of various concentrations of drugs for 48 h and treated with a Cell Titer-Blue reagent for 4 h at 37 °C. The fluorescent signals were recorded at $530/25_{excitation}$ and $590/35_{emission}$ using Bio Tek microplate reader.

5.2.4. Virus Infectivity Assay. Virus stocks were prepared by transfecting HEK-293T cells with 5 μg of HIV-1 subtype B NL43 viral plasmid in the presence of porphyrins and 5% DMSO in water solvent was used as a control (−). After 48 h of transfection, the virus culture supernatant was collected, centrifuged at 845g for 5 min to remove cellular debris, and filtered through 0.45 μm pore-sized filter disc to remove cellular contaminants. The viral titer was estimated by HIV-1 p24 ELISA (Micro ELISA kit-J Mitra and Co). For the determination of virus infectivity, a single-round infectivity assay was performed. Ten ng of HIV-1 p24 equiv virus was used to infect TZM-bl cells (5×10^4 cells/well) in the presence of 20 μg DEAE-dextran per mL in a 24-well plate. Luciferase activity was measured 48 h postinfection using a steady-Glo luciferase assay kit (Promega) as per the manufacturer's recommendations.

5.2.5. Entry Inhibition Assays in Non-PDT Conditions. Virus stocks of HIV-1 subtype B NL4−3 viruses were produced in HEK-293T cells. The viral supernatant was collected 24 h post-transfection, centrifuged, and filtered to remove residual cell debris. The virus was quantified using an HIV-1 p24 Antigen Capture ELISA kit. HIV-1 p24 normalized virus was used to infect TZM-bl cells (7×10^4/well) in the presence of 20 μg DEAE-dextran per mL. Two different conditions were employed for the infection; (A) The compounds were added to the cells during virus infection. (B) The compounds were added to the cells postviral infection and maintained for 48 h. HIV-1 fusion inhibitor T-20 was used as a positive control. After 48 h of infection, the luciferase activity in the cell lysates was measured using the Steady-Glo luciferase assay kit (Promega) following the manufacturer's recommendations. Percentage relative entry was calculated by normalizing the luciferase units with respect to control 5% DMSO-water (−) samples.

5.2.6. Antiviral Activity in Photodynamic Conditions (PDT). For PDT experiments, we designed a light box consisting of an arrangement of two light source lamps (36W/4P fluorescent lamp). The cells were treated from a fixed distance of 6 in. for 45 min from above in all PDT experiments. The effect of porphyrins on HIV-1 entry or infection in the presence of light, and on HIV-1 production in infected cells was explored.

The effect of porphyrins on cell viability/cytotoxicity was performed on TZM-bl cells using Cell Titer-Blue Assay (Promega) as per the manufacturer's recommendation as explained above. Next, the photoinhibitory effect of porphyrins on HIV-1 infection was determined. For this, 10 ng of HIV-1 p24 equiv HIV-1 subtype B NL4−3 virus was pretreated with porphyrins followed by light irradiation inside the light box. This pretreated virus was then used to infect TZM-bl cells for 2 h at 37 °C. Postinfection cells were washed and incubated in the absence of porphyrins for 48 h. Relative luminescence corresponding to HIV entry and infection was measured compared to control (−) (5% DMSO in water). Then, we evaluated the effect of porphyrins on HIV-1 production in infected cells when added postviral infection. Briefly, at first TZM-bl cells were infected with 10 ng of HIV-1 p24 equiv subtype B NL4−3 virus for 2 h at 37 °C. Postinfection, the porphyrins were added along with fresh media and exposed to light irradiation inside the light box. These treated cells were then incubated at 37 °C for 48 h and relative luminescence corresponding to HIV production inside the cells was measured compared to control (−)(5% DMSO in water).

5.3. Antibacterial Activity through Disc Diffusion. *5.3.1. Antimicrobial Activity. 5.3.1.1. Microbial Growth Conditions.* For the antimicrobial activity the Luria−Bertani (LB) and Nutrient Medium (NM), along with their respective growth media constituents, were procured from HI Media. The type strains *E. coli* ATCC 25922 and *S. aureus* ATCC 25923 were sourced from the Department of Microbiology's culture collection. The nutrient agar plates and the Luria−Bertani were prepared using a standard protocol. A disinfected wire loop was used to streak the stock bacterial strain onto the medium. After transferring the cultured microorganism, the plates were placed in an incubator oven at 37 ± 1 °C for 24−48 h. The strains were preserved on Nutrient Agar (NA) slants at −20 °C. They were then revitalized in Luria−Bertani (LB) broth and subjected to subculturing at regular intervals.

5.3.1.2. Disc Diffusion Assay. Bacterial sensitivity to the antibacterial compounds was evaluated using a disc diffusion assay with disks impregnated with the compounds. In this study, disk porphyrin compounds were utilized. The filter paper loaded with porphyrin compounds was dried at room temperature, and uniform disks (5 mm in diameter) containing 0.5, 1, and 2 μM of **P_3AmZM**, **c-P_2Am_2ZM**, **PAm_3M**, **PAm_3ZM**, **c-P_2Am_2M**, **P_3AmM**, **TMPyPZ**, and **TMPy**, respectively, were punched out and stored in a desiccator at room temperature. A sterile swab was used to uniformly apply the bacterial suspension to the surface of a nutrient agar plate before placing the disks on the plate (four disks per plate). The bacterial density was adjusted in sterile PBS solution to achieve a concentration of 10^8−10^9 CFU/mL, as determined by measuring absorbance at 600 nm according to McFarland

https://doi.org/10.1021/acsomega.4c09535
ACS Omega 2025, 10, 22482−22507

standards. The plates were incubated at 37 °C for 24 h. One set of plates was kept in darkness, while the other set was exposed to light for 30 min before incubation. After incubation, the average diameter of the zones of inhibition (ZOI) around the disks was measured using a ruler with 1 mm resolution.

5.3.2. MIC Estimation. The minimum inhibitory concentration (MIC) is defined as the lowest concentration of a material that inhibits the growth of microorganisms. In this study, MIC was determined using batch cultures containing various concentrations of porphyrin compounds in suspension, following the procedure described by Li et al.[74] Initially, all bacterial strains were cultured and harvested by centrifugation at 8000*g* and 4 °C for 10 min. The cells were washed three times in PBS (0.2 mol/L, pH 7.4) and resuspended to achieve a final concentration of 10^{-8} cells/mL in PBS. These resuspended cells were then inoculated into 1 mL of fresh medium supplemented with different concentrations of compounds. The cultures were incubated in an orbital shaker at 200 rpm and 37 °C for 24 h. Bacterial growth was measured by determining the absorbance at 600 nm using a spectrophotometer (Thermo Spectronic, Helios Epsilon). The experiments included a positive control (flask containing porphyrin compounds and nutrient medium without bacterial inoculum) and a negative control (flask containing bacterial inoculum and nutrient medium without porphyrin compounds). All experiments were conducted in triplicate. The bactericidal effect of porphyrin compounds at different concentrations was tested using all the microbial cultures selected for the study.

MIC values of the porphyrin compounds against the bacterial isolates are listed in Table S7. The antimicrobial activity was found to be higher in **c-P_2Am_2M**, **c-P_2Am_2ZM**, **P_3AmZM**, **P_3AmM**, and **PAm_3ZM** compounds ($P < 0.05$). The results suggest that the antimicrobial activity was more prominent after light exposure.

5.3.3. Minimum Bactericidal Concentration (MBC). The Minimum Bactericidal Concentration (MBC) is defined as the lowest concentration of an antimicrobial agent that results in a 3-logarithmic reduction (99.9% killing) in the number of viable bacterial cells from the initial inoculum. The MBC test is a robust method used to compare the bactericidal activity of different antimicrobial agents. The dose-dependent killing activity of different concentrations of porphyrin compounds against *E. coli* and *S. aureus* (in 20 mL PBS inoculated with 10^8−10^9 CFU/mL of cells) was determined. The bacterial cells were initially grown in Nutrient Broth (NB) medium at 37 °C for 24 h with continuous agitation. Cells in the late log phase were harvested by centrifugation at 10,000 rpm for 10 min, washed three times by centrifugation (10,000 rpm for 10 min), and resuspended in PBS (1.0 M, pH 8.0). The cell suspension was diluted in sterile PBS to achieve a concentration of 10^8−10^9 CFU/mL, adjusted by measuring absorbance at 600 nm according to McFarland standards and further verified by plating and enumerating CFU on nutrient agar plates. Various concentrations of porphyrin compounds were added to the PBS suspensions of bacterial cells. Culture samples were collected at intervals from 0 to 240 min of incubation and spread onto Nutrient Agar (NA) plates.

Colony-forming units (CFU) were counted after incubation at 37 °C for 24 h, and the percentage decrease in the cell population was determined. The viable cell count of the test organisms was estimated in parallel in a control experiment without any porphyrin compounds.

5.3.4. Statistical Analysis. All the experiments were performed in duplicates. The experimental data for the MIC and MBC assays were statistically analyzed. The standard error of the mean was calculated using standard procedures. Significance was determined using an independent *t* test with a threshold of $P < 0.05$, conducted with SPSS 16 software. Population densities of the isolates were further estimated using logarithmic transformation.

5.4. Molecular Docking Procedure. Docking simulations were executed to evaluate the binding affinities and molecular interactions, to understand the structural mechanisms responsible for the in vitro antiretroviral effects of the compounds.

Docking simulations were conducted using AutoDock VINA integrated into the PyRx 0.8[1] virtual screening tool to identify compounds with high binding affinity. In silico docking studies were performed to evaluate the molecular interactions of the compounds with HIV gp120 (PDB: 8FM5)[2] protease (PDB: 2PSV),[3] and reverse transcriptase (PDB: 7OT6)[4] proteins, with cocrystallized inhibitors Y2E, MUV, and 1l4, respectively.

In our current docking investigation, our main focus was on exploring several well-known HIV targets, to uncover molecular interactions and gain structural-based mechanistic insights into these compounds.

The protein structure was prepared to ensure an optimized configuration for docking studies using the UCSF Chimera Dock Prep module. This process involved several steps: removal of water molecules and other ligands, addition of missing atoms and residues, energy minimization, and assignment of charges and polar hydrogens. Subsequently, the prepared structure was converted to the pdbqt format.

The 2D structures of the ligands were drawn using ChemDraw software. These structures were then optimized through energy minimization, employing MMFF94 force field parameters and a conjugate gradient algorithm via the Open Babel module of PyRx. Subsequently, the ligands were converted to the AutoDock-compatible pdbqt format to facilitate docking exploration.

Postdocking analysis and visualization of binding poses and molecular interactions were conducted using BIOVIA Discovery Studio 2021 and Chimera X tools.[5] The Autodock Vina grid box was positioned around the active site of the antagonist, outlining the search space with the parameters summarized in Table S8.

In the docking program's validation process, Y2E was meticulously redocked into its cocrystallized site on the HIV gp120 protein. A notably low Root Mean Square Deviation (RMSD) value of 1.53 Å was noted between the docked and native poses. This result serves as compelling evidence of the program's ability to accurately predict the binding poses of inhibitors within HIV proteins. This demonstrates the program's capability to reproduce the spatial positioning of Y2E within its designated binding site, affirming the docking algorithm's reliability and precision. The binding energies and molecular interaction profiles of the compounds were compared with those of cocrystallized ligands and drugs targeting various HIV targets. These targets play crucial roles in different stages of the viral life cycle: viral entry (gp120), production of infectious virions (protease), and replication (reverse transcriptase).

https://doi.org/10.1021/acsomega.4c09535
ACS Omega 2025, 10, 22482−22507

■ ASSOCIATED CONTENT

Data Availability Statement

All data generated or analyzed during this study are included in this published article [and its Supporting Information files].

Supporting Information

The Supporting Information is available free of charge at https://pubs.acs.org/doi/10.1021/acsomega.4c09535.

Experimental details: synthetic methods, details of biological assays employed, characterization data: ^{1}H NMR, and mass spectral data (PDF)

■ AUTHOR INFORMATION

Corresponding Authors

Piyush Pandey − *Department of Microbiology, Assam University, Silchar 788011 Assam, India;* orcid.org/0000-0003-3175-0122; Email: piyushddn@gmail.com

Ritu Gaur − *Faculty of Life Sciences and Biotechnology, South Asian University, New Delhi 110021, India*; Email: rgaur@sau.ac.in

Devashish Sengupta − *Department of Chemistry, Assam University, Silchar 788011 Assam, India;* orcid.org/0000-0001-7512-8664; Email: devashish.sengupta@uni.sydney.edu.au

Authors

Debdulal Sharma − *Department of Chemistry, Assam University, Silchar 788011 Assam, India;* orcid.org/0000-0003-2708-8084

Madhu Rai − *Faculty of Life Sciences and Biotechnology, South Asian University, New Delhi 110021, India*

Nandita Das − *Department of Microbiology, Assam University, Silchar 788011 Assam, India*

Ravi Kumar Kapavarapu − *Department of Pharmaceutical Chemistry and Phytochemistry, Nirmala College of Pharmacy, Mangalgiri 522503 Andhra Pradesh, India*

Complete contact information is available at: https://pubs.acs.org/10.1021/acsomega.4c09535

Author Contributions

D.S. carried out the synthesis, isolation, and characterization of the porphyrins and contributed to compiling the synthetic, photochemical, and photophysical aspects presented in the paper. M.R. performed the experiments and data analysis for the antiviral studies. M.R., guided by R.G., wrote the antiviral section. N.D. carried out the antibacterial and antibiofilm assays under the supervision of P.P. N.D., guided by P.P., wrote the antibacterial section presented in the manuscript. P.P. designed the antibacterial studies and antibiofilm assays. R.K. conducted the in silico evaluation of compounds with HIV targets. R.G. designed and supervised the anti-HIV studies and contributed to writing the anti-HIV part of the manuscript. D.S. supervised and coordinated the project, conceptualized the design, synthesis, and application of the compounds as anti-HIV-1 and antibacterial agents, and contributed to data analysis, availing funds for the project, consolidation, and writing of the manuscript.

Funding

The support by DBT (Nanobiotechnology) Project Reg. No: BT/PR25024/NER/95/961/2017, granted to Devashish Sengupta from the Government of India, Ministry of Science and Technology; Department of Biotechnology is acknowledged.

Notes

The authors declare no competing financial interest.

■ ACKNOWLEDGMENTS

The authors gratefully acknowledge STIC-SAIF, Kochi for ^{1}H NMR and mass spectral analysis and CDRI, Lucknow, for HRMS spectra. The authors acknowledge the invaluable assistance provided by Aradhana Singh, Faculty of Life Science and Biotechnology, South Asian University, and Pushkar Rai, Department of Chemistry, Assam University, throughout all stages of the preparation of this research work.

■ REFERENCES

(1) Pavani, C.; Uchoa, A. F.; Oliveira, C. S.; Iamamoto, Y.; Baptista, M. S. Effect of zinc insertion and hydrophobicity on the membrane interactions and PDT activity of porphyrin photosensitizers. *Photochem. Photobiol. Sci.* **2009**, *8* (2), 233−240.

(2) Deda, D. K.; Uchoa, A. F.; Caritá, E.; Baptista, M. S.; Toma, H. E.; Araki, K. A new micro/nanoencapsulated porphyrin formulation for PDT treatment. *Int. J. Pharm.* **2009**, *376* (1−2), 76−83.

(3) Villanueva, A.; Jori, G. Pharmacokinetic and tumour-photosensitizing properties of the cationic porphyrin meso-tetra (4N-methylpyridyl) porphine. *Cancer Lett.* **1993**, *73* (1), 59−64.

(4) McCormick, B. P. P.; Pansa, M. F.; Sanabria, L. N. M.; Carvalho, C. M.; Faustino, M. A. F.; Neves, M. G. P.; Cavaleiro, J. A.; Vittar, N. B. R.; Rivarola, V. A. Cationic porphyrin derivatives for application in photodynamic therapy of cancer. *Laser Phys.* **2014**, *24* (4), No. 045603.

(5) Stallivieri, A.; Le Guern, F.; Vanderesse, R.; Meledje, E.; Jori, G.; Frochot, C.; Acherar, S. Synthesis and photophysical properties of the photoactivatable cationic porphyrin 5-(4-N-dodecylpyridyl)-10, 15, 20-tri (4-N-methylpyridyl)-21H, 23H-porphyrin tetraiodide for anti-malaria PDT. *Photochem. Photobiol. Sci.* **2015**, *14* (7), 1290−1295.

(6) Malatesti, N.; Munitic, I.; Jurak, I. Porphyrin-based cationic amphiphilic photosensitisers as potential anticancer, antimicrobial and immunosuppressive agents. *Biophys. Rev.* **2017**, *9* (2), 149−168.

(7) Mazumdar, Z. H.; Sharma, D.; Mukherjee, A.; Basu, S.; Shukla, P. K.; Jha, T.; Sengupta, D. meso-Thiophenium Porphyrins and Their Zn (II) Complexes: A New Category of Cationic Photosensitizers. *ACS Med. Chem. Lett.* **2020**, *11* (10), 2041−2047.

(8) Sengupta, D.; Rai, M.; Mazumdar, Z. H.; Sharma, D.; Singha, K. M.; Pandey, P.; Gaur, R. Two cationic meso-thiophenium porphyrins and their zinc-complexes as anti-HIV-1 and antibacterial agents under non-photodynamic therapy (PDT) conditions. *Bioorg. Med. Chem. Lett.* **2022**, *65*, No. 128699.

(9) Sengupta, D.; Timilsina, U.; Mazumder, Z. H.; Mukherjee, A.; Ghimire, D.; Markandey, M.; Upadhyaya, K.; Sharma, D.; Mishra, N.; Jha, T.; et al. Dual activity of amphiphilic Zn (II) nitroporphyrin derivatives as HIV-1 entry inhibitors and in cancer photodynamic therapy. *Eur. J. Med. Chem.* **2019**, *174*, 66−75.

(10) Sun, R. W. Y.; Yu, W. Y.; Sun, H.; Che, C. M. In Vitro Inhibition of Human Immunodeficiency Virus Type-1 (HIV-1) Reverse Transcriptase by Gold (iii) Porphyrins. *ChemBioChem* **2004**, *5* (9), 1293−1298.

(11) Vzorov, A. N.; Dixon, D. W.; Trommel, J. S.; Marzilli, L. G.; Compans, R. W. Inactivation of human immunodeficiency virus type 1 by porphyrins. *Antimicrob. Agents Chemother.* **2002**, *46* (12), 3917−3925.

(12) Spesia, M. B.; Lazzeri, D.; Pascual, L.; Rovera, M.; Durantini, E. N. Photoinactivation of *Escherichia coli* using porphyrin derivatives with different number of cationic charges. *FEMS Immunol. Med. Microbiol.* **2005**, *44* (3), 289−295.

(13) Modica-Napolitano, J. S.; Aprille, J. R. Delocalized lipophilic cations selectively target the mitochondria of carcinoma cells. *Adv. Drug Delivery Rev.* **2001**, *49* (1−2), 63−70.

(14) Kou, J.; Dou, D.; Yang, L. Porphyrin photosensitizers in photodynamic therapy and its applications. *Oncotarget* **2017**, *8* (46), 81591−81603.

(15) Jones, R. N. Resistance Patterns Among Nosocomial Pathogens: Trends Over the Past Few Years. *Chest* **2001**, *119* (2), 397S−404S.
(16) Sabino, C. P.; Wainwright, M.; Ribeiro, M. S.; Sellera, F. P.; dos Anjos, C.; da Silva Baptista, M.; Lincopan, N. Global priority multidrug-resistant pathogens do not resist photodynamic therapy. *J. Photochem. Photobiol., B* **2020**, *208*, No. 111893.
(17) Yu, C.; Sui, S.; Yu, X.; Huang, W.; Wu, Y.; Zeng, X.; Chen, Q.; Wang, J.; Peng, Q. Ti3C2Tx MXene loaded with indocyanine green for synergistic photothermal and photodynamic therapy for drug-resistant bacterium. *Colloids Surf., B* **2022**, *217*, No. 112663.
(18) Boluki, E.; Pourhajibagher, M.; Bahador, A. The combination of antimicrobial photocatalysis and antimicrobial photodynamic therapy to eradicate the extensively drug-resistant colistin resistant Acinetobacter baumannii. *Photodiagn. Photodyn. Ther.* **2020**, *31*, No. 101816.
(19) Böhm, H.; Banner, D.; Bendels, S.; Kansy, M.; Kuhn, B.; Müller, K.; Obst-Sander, U.; Stahl, M. Fluorine in medicinal chemistry. *ChemBioChem* **2004**, *5* (5), 637−643.
(20) Stockert, J. C.; Vanzulli, S. I.; Canete, M.; Villanueva, A.; Juarranz, A.; Nonell, S.; Colombo, L. L. Regression of the murine LM3 tumor by repeated photodynamic therapy with meso-tetrakis-(4-N, N, N-trimethylanilinium) porphine. *J. Porphyrins Phthalocyanines* **2009**, *13* (04n05), 560−566.
(21) Colombo, L.; Juarranz, A.; Cañete, M.; Villanueva, A.; Stockert, J. Photodynamic therapy of the murine LM3 tumor using meso-tetra (4-N, N, N-trimethylanilinium) Porphine. *Int. J. Biomed. Sci.* **2007**, *3* (4), 258−262.
(22) Cohen, B. A.; Kaloyeros, A. E.; Bergkvist, M. Nucleotide-driven packaging of a singlet oxygen generating porphyrin in an icosahedral virus. *J. Porphyrins Phthalocyanines* **2012**, *16* (01), 47−54.
(23) Hancock, R. E. W.; Bell, A.Antibiotic Uptake into Gram-negative Bacteria. In *Perspectives in Antiinfective Therapy*; Springer, 1989; pp 42−53.
(24) Seferyan, M. A.; Saverina, E. A.; Frolov, N. A.; Detusheva, E. V.; Kamanina, O. A.; Arlyapov, V. A.; Ostashevskaya, I. I.; Ananikov, V. P.; Vereshchagin, A. N. Multicationic Quaternary Ammonium Compounds: A Framework for Combating Bacterial Resistance. *ACS Infect. Dis.* **2023**, *9* (6), 1206−1220.
(25) Alenezi, K.; Tovmasyan, A.; Batinic-Haberle, I.; Benov, L. T. Optimizing Zn porphyrin-based photosensitizers for efficient antibacterial photodynamic therapy. *Photodiagn. Photodyn. Ther.* **2017**, *17*, 154−159.
(26) Stojiljkovic, I.; Evavold, B. D.; Kumar, V. Antimicrobial properties of porphyrins. *Expert Opin. Invest. Drugs* **2001**, *10* (2), 309−320.
(27) Tovmasyan, A.; Batinic-Haberle, I.; Benov, L. Antibacterial Activity of Synthetic Cationic Iron Porphyrins. *Antioxidants* **2020**, *9* (10), No. 972.
(28) Li, X.; Su, Z.; Fujitsuka, M.; Osakada, Y. Zinc porphyrin covalent organic nanodisks synthesized from covalent organic frameworks and their photocatalytic antibacterial activity. *JCIS Open* **2023**, *10*, No. 100083.
(29) Garcia-Sampedro, A.; Tabero, A.; Mahamed, I.; Acedo, P. Multimodal use of the porphyrin TMPyP: From cancer therapy to antimicrobial applications. *J. Porphyrins Phthalocyanines* **2019**, *23*, 11−27.
(30) Tománková, K. B.; Opletalová, A.; Poláková, K.; Kalytchuk, S.; Jiravová, J.; Malohlava, J.; Malina, L.; Kolářová, H. Size-selected graphene oxide loaded with photosensitizer (TMPyP) for targeting photodynamic therapy in vitro. *Processes* **2020**, *8* (2), No. 251.
(31) Acedo, P.; Stockert, J.; Cañete, M.; Villanueva, A. Two combined photosensitizers: a goal for more effective photodynamic therapy of cancer. *Cell Death Dis.* **2014**, *5* (3), No. e1122.
(32) Malara, D.; Høj, L.; Oelgemöller, M.; Malerba, M.; Citarrella, G.; Heimann, K. Sensitivity of live microalgal aquaculture feed to singlet oxygen-based photodynamic therapy. *J. Appl. Phycol.* **2019**, *31* (6), 3593−3606.
(33) Beyene, B. B.; Wassie, G. A. Antibacterial activity of Cu(II) and Co(II) porphyrins: role of ligand modification. *BMC Chem.* **2020**, *14* (1), No. 51.
(34) de Carvalho Ferreira, D.; da Silva, G. R.; Cavalcante, F. S.; do Carmo, F. L.; Fernandes, L. A.; Moreira, S.; Passos, M. R. L.; Colombo, A. P. V.; dos Santos, K. R. N. Methicillin-resistant Staphylococcus aureus in HIV patients: risk factors associated with colonization and/or infection and methods for characterization of isolates-a systematic review. *Clinics* **2014**, *69*, 770−776.
(35) Ambrogio, F.; Meduri, A. R.; Infante, G.; Poli, M. A.; Romita, P.; Bonamonte, D.; Filotico, R.; Ingravallo, G.; Cazzato, G.; Laface, C.; et al. Photodynamic Therapy Used to Treat an HIV Patient with an Efflorescence of Viral Warts after HAART Therapy. *Diagnostics* **2023**, *13* (6), No. 1098.
(36) Yang, R.; Bi, X.-D.; Li, Y.; Liu, M.; Hu, M.-Q.; Zhao, L.-M.; Zhang, H.; Gao, F. Scorpion-Shaped Zinc Porphyrins as Tetrafunctional TAR RNA Predators and HIV-1 Reverse Transcriptase Inhibitors. *Inorg. Chem.* **2022**, *61* (28), 10774−10780.
(37) Wong, S.-Y.; Sun, R. W.-Y.; Chung, N. P.-Y.; Lin, C.-L.; Che, C.-M. Physiologically stable vanadium (IV) porphyrins as a new class of anti-HIV agents. *Chem. Commun.* **2005**, No. 28, 3544−3546.
(38) Dixon, D. W.; Kim, M. S.; Kumar, V.; Obara, G.; Marzilli, L. G.; Schinazi, R. F. Amino-and hydroxytetraphenylporphyrins with activity against the human immunodeficiency virus. *Antiviral Chem. Chemother.* **1992**, *3* (5), 279−282.
(39) Lebedeva, N. S.; Gubarev, Y. A.; Koifman, M. O.; Koifman, O. I. The application of porphyrins and their analogues for inactivation of viruses. *Molecules* **2020**, *25* (19), No. 4368.
(40) Kubát, P.; Lang, K.; Cígler, P.; Kožíšek, M.; Matějíček, P.; Janda, P.; Zelinger, Z.; Prochazka, K.; Král, V. Tetraphenylporphyrin-cobalt (III) bis (1, 2-dicarbollide) conjugates: from the solution characteristics to inhibition of HIV protease. *J. Phys. Chem. B* **2007**, *111* (17), 4539−4546.
(41) DeCamp, D. L.; Babe, L. M.; Salto, R.; Lucich, J. L.; Koo, M. S.; Kahl, S. B.; Craik, C. S. Specific inhibition of HIV-1 protease by boronated porphyrins. *J. Med. Chem.* **1992**, *35* (18), 3426−3428.
(42) Schaeck, J. J. *The Synthesis of Boronated Porphyrins as Inhibitors of HIV-1 Protease*; University of California: San Francisco, 1997.
(43) Rundstadler, T.; Mothes, E.; Amrane, S.; Stigliani, J.-L.; Verhaeghe, P.; Pratviel, G. Gold(III) porphyrins: Synthesis and interaction with G-quadruplex DNA. *J. Inorg. Biochem.* **2021**, *223*, No. 111551.
(44) Amrane, S.; Andreola, M.-a.; Pratviel, G.; Mergny, J.-L. Derivatives of Porphyrins, Their Process of Preparation and Their Use for Treating Viral Infections. U.S. Patent US10577375B2, 2020.
(45) Fonteh, P. N.; Keter, F. K.; Meyer, D. HIV therapeutic possibilities of gold compounds. *BioMetals* **2010**, *23* (2), 185−196.
(46) Bullous, A. *Development of Porphyrin-antiangiogenic Antibody Immunoconjugates for Photodynamic Therapy*; University of Hull, 2010.
(47) Wang, C.; Wamser, C. C. Hyperporphyrin Effects in the Spectroscopy of Protonated Porphyrins with 4-Aminophenyl and 4-Pyridyl Meso Substituents. *J. Phys. Chem. A* **2014**, *118* (20), 3605−3615.
(48) Wang, C.; Wamser, C. C. NMR Study of Hyperporphyrin Effects in the Protonations of Porphyrins with 4-Aminophenyl and 4-Pyridyl Meso Substituents. *J. Org. Chem.* **2015**, *80* (15), 7351−7359.
(49) Szurko, A.; Krämer-Marek, G.; Wideł, M.; Ratuszna, A.; Habdas, J.; Kuś, P. Photodynamic effects of two water soluble porphyrins evaluated on human malignant melanoma cells in vitro. *Acta Biochim. Pol.* **2003**, *50* (4), 1165−1174.
(50) Boyle, R. W.; Clarke, O. J.; Sutton, J. M.; Greenman, J. Chromophores. U.S. Patent US2003O2, 2003.
(51) Khurana, B.; Ouk, T.-S.; Lucas, R.; Senge, M. O.; Sol, V. Photosensitizer-hyaluronic acid complexes for antimicrobial photodynamic therapy (aPDT). *J. Porphyrins Phthalocyanines* **2022**, *26* (08n09), 585−593.
(52) Antonangelo, A. R.; Westrup, K. C. M.; Burt, L. A.; Bezzu, C. G.; Malewschik, T.; Machado, G. S.; Nunes, F. S.; McKeown, N. B.; Nakagaki, S. Synthesis, crystallographic characterization and homoge-

https://doi.org/10.1021/acsomega.4c09535
ACS Omega 2025, 10, 22482−22507

neous catalytic activity of novel unsymmetric porphyrins. *RSC Adv.* **2017**, *7* (80), 50610−50618.
(53) Dechan, P.; Devi Bajju, G.; Sood, P. Trans A2B2 Porphyrins: Synthesis, Crystal Structure Determinations and Hirshfeld Surface Analysis. *ChemistrySelect* **2020**, *5* (24), 7298−7309.
(54) Mazumder, Z. H. *Water-soluble, Meso-substituted, Free-base and Metallated Thiophenium and/or Pyridinium and/or Indole Derivatives of Porphyrin: Their Role as Photosensitizers*; Assam University: Silchar, 2017.
(55) Sengupta, D. *Synthesis, Characterisation and Biological Activities of Singly and Doubly Linked Water-soluble Porphyrin-fulleropyrrolidine Dyads*; University of Sydney, 2006.
(56) Elkihel, A.; Vernisse, C.; Ouk, T.-S.; Lucas, R.; Chaleix, V.; Sol, V. Cationic porphyrin−xylan conjugate hydrogels for photodynamic antimicrobial chemotherapy. *J. Appl. Polym. Sci.* **2022**, *139* (38), No. e52744.
(57) Cheng, R.-J.; Chen, P.-Y.; Lovell, T.; Liu, T.; Noodleman, L.; Case, D. A. Symmetry and Bonding in Metalloporphyrins. A Modern Implementation for the Bonding Analyses of Five- and Six-Coordinate High-Spin Iron(III)−Porphyrin Complexes through Density Functional Calculation and NMR Spectroscopy. *J. Am. Chem. Soc.* **2003**, *125* (22), 6774−6783.
(58) Fagadar-Cosma, E.; Mirica, M. C.; Balcu, I.; Bucovicean, C.; Cretu, C.; Armeanu, I.; Fagadar-Cosma, G. Syntheses, spectroscopic and AFM characterization of some manganese porphyrins and their hybrid silica nanomaterials. *Molecules* **2009**, *14* (4), 1370−1388.
(59) Valicsek, Z.; Horváth, O.; Stevenson, K. L. Photophysics and photochemistry of water-soluble, sitting-atop bis-thallium (I) 5, 10, 15, 20-tetrakis (4-sulfonatophenyl) porphyrin. *Photochem. Photobiol. Sci.* **2004**, *3* (7), 669−673.
(60) Gouterman, M. Spectra of porphyrins. *J. Mol. Spectrosc.* **1961**, *6*, 138−163.
(61) Myśliwa-Kurdziel, B.; Solymosi, K.; Kruk, J.; Böddi, B.; Strzałka, K. Solvent effects on fluorescence properties of protochlorophyll and its derivatives with various porphyrin side chains. *Eur. Biophys. J.* **2008**, *37* (7), 1185−1193.
(62) de Jong, M.; Seijo, L.; Meijerink, A.; Rabouw, F. T. Resolving the ambiguity in the relation between Stokes shift and Huang-Rhys parameter. *Phys. Chem. Chem. Phys.* **2015**, *17* (26), 16959−16969.
(63) Mazumder, Z. H.; Sharma, D.; Sengupta, D.; Mukherjee, A.; Boruah, J. S.; Basu, S.; Shukla, P. K.; Jha, T. Photodynamic activity attained through raptured p-conjugation of pyridyl groups with a porphyrin macrocycle: Synthesis, Photophysical and Photobiological Evaluation of 5-mono-(4-nitrophenyl)-10,15,20-tris-[4-(phenoxymethyl)pyridine]porphyrin and its Zn(II) complex. *Photochem. Photobiol. Sci.* **2020**, *19*, 1776−1789.
(64) Jaung, J.-Y. Synthesis of new porphyrins with dicyanopyrazine moiety and their optical properties. *Dyes Pigm.* **2007**, *72* (3), 315−321.
(65) Zhang, L.; Huang, Z.; Dai, D.; Xiao, Y.; Lei, K.; Tan, S.; Cheng, J.; Xu, Y.; Liu, J.; Qian, X. Thio-bisnaphthalimides as heavy-atom-free photosensitizers with efficient singlet oxygen generation and large stokes shifts: synthesis and properties. *Org. Lett.* **2016**, *18* (21), 5664−5667.
(66) Zems, Y.; Moiseev, A. G.; Perepichka, D. F. Convenient synthesis of a highly soluble and stable phosphorescent Platinum porphyrin dye. *Org. Lett.* **2013**, *15* (20), 5330−5333.
(67) Zhang, D.-W.; Chen, W.-T. Two novel tcpp porphyrinic compounds: in situ syntheses, characterization and reaction mechanism. *J. Chil. Chem. Soc.* **2017**, *62* (1), 3381−3385.
(68) De Paoli, V. M.; De Paoli, S. H.; Borissevitch, I. E.; Tedesco, A. C. Fluorescence lifetime and quantum yield of TMPyPH2 associated with micelles and DNA. *J. Alloys Compd.* **2002**, *344* (1), 27−31.
(69) Gonçalves, P.; Franzen, P. L.; Correa, D. S.; Almeida, L. M.; Takara, M.; Ito, A. S.; Zílio, S. C.; Borissevitch, I. E. Effects of environment on the photophysical characteristics of mesotetrakis methylpyridiniumyl porphyrin (TMPyP). *Spectrochim. Acta, Part A* **2011**, *79* (5), 1532−1539.
(70) Mahajan, P. G.; Dige, N. C.; Vanjare, B. D.; Eo, S.-H.; Seo, S.-Y.; Kim, S. J.; Hong, S.-K.; Choi, C.-S.; Lee, K. H. A potential mediator for photodynamic therapy based on silver nanoparticles functionalized with porphyrin. *J. Photochem. Photobiol., A* **2019**, *377*, 26−35.
(71) Mahajan, P. G.; Dige, N. C.; Vanjare, B. D.; Kim, C.-H.; Seo, S.-Y.; Lee, K. H. Design and synthesis of new porphyrin analogues as potent photosensitizers for photodynamic therapy: spectroscopic approach. *J. Fluoresc.* **2020**, *30* (2), 397−406.
(72) Mahajan, P. G.; Dige, N. C.; Vanjare, B. D.; Phull, A. R.; Kim, S. J.; Hong, S.-K.; Lee, K. H. Synthesis, photophysical properties and application of new porphyrin derivatives for use in photodynamic therapy and cell imaging. *J. Fluoresc.* **2018**, *28* (4), 871−882.
(73) Platt, E. J.; Wehrly, K.; Kuhmann, S. E.; Chesebro, B.; Kabat, D. Effects of CCR5 and CD4 cell surface concentrations on infections by macrophagetropic isolates of human immunodeficiency virus type 1. *J. Virol.* **1998**, *72* (4), 2855−2864.
(74) Checkley, M. A.; Luttge, B. G.; Mercredi, P. Y.; Kyere, S. K.; Donlan, J.; Murakami, T.; Summers, M. F.; Cocklin, S.; Freed, E. O. Reevaluation of the requirement for TIP47 in human immunodeficiency virus type 1 envelope glycoprotein incorporation. *J. Virol.* **2013**, *87* (6), 3561−3570.
(75) Matthews, T.; Salgo, M.; Greenberg, M.; Chung, J.; DeMasi, R.; Bolognesi, D. Enfuvirtide: the first therapy to inhibit the entry of HIV-1 into host CD4 lymphocytes. *Nat. Rev. Drug Discovery* **2004**, *3* (3), 215−225.
(76) Sengupta, D.; Das, S.; Sharma, D.; Chattopadhyaya, S.; Mukherjee, A.; Mazumdar, Z. H.; Das, B.; Basu, S.; Sengupta, M. An Anti-inflammatory Fe3O4-Porphyrin Nanohybrid Capable of Apoptosis through Upregulation of p21 Kinase Inhibitor Having Immunoprotective Properties under Anticancer PDT Conditions. *ChemMedChem* **2022**, *17* (2), No. e202100550.
(77) Zhou, Z.-X.; Gao, F.; Chen, X.; Tian, X.-J.; Ji, L.-N. Selective Binding and Reverse Transcription Inhibition of Single-Strand poly(A) RNA by Metal TMPyP Complexes. *Inorg. Chem.* **2014**, *53* (19), 10015−10017.
(78) Batishchev, O. V.; Kalutskii, M. A.; Varlamova, E. A.; Konstantinova, A. N.; Makrinsky, K. I.; Ermakov, Y. A.; Meshkov, I. N.; Sokolov, V. S.; Gorbunova, Y. G. Antimicrobial activity of photosensitizers: arrangement in bacterial membrane matters. *Front. Mol. Biosci.* **2023**, *10*, No. 1192794.
(79) Hashimoto, M. C. E.; Prates, R. A.; Kato, I. T.; Núñez, S. C.; Courrol, L. C.; Ribeiro, M. S. Antimicrobial photodynamic therapy on drug-resistant Pseudomonas aeruginosa-induced infection. An in vivo study. *Photochem. Photobiol.* **2012**, *88* (3), 590−595.
(80) Orenstein, A.; Klein, D.; Kopolovic, J.; Winkler, E.; Malik, Z.; Keller, N.; Nitzan, Y. The use of porphyrins for eradication of Staphylococcus aureus in burn wound infections. *FEMS Immunol. Med. Microbiol.* **1997**, *19* (4), 307−314.
(81) Malik, Z.; Ladan, H.; Nitzan, Y. Photodynamic inactivation of Gram-negative bacteria: Problems and possible solutions. *J. Photochem. Photobiol., B* **1992**, *14* (3), 262−266.
(82) Agnihotri, S.; Mukherji, S.; Mukherji, S. Size-controlled silver nanoparticles synthesized over the range 5−100 nm using the same protocol and their antibacterial efficacy. *RSC Adv.* **2014**, *4* (8), 3974−3983.
(83) Valduga, G.; Breda, B.; Giacometti, G. M.; Jori, G.; Reddi, E. Photosensitization of Wild and Mutant Strains of*Escherichia coli*bymeso-Tetra (N-methyl-4-pyridyl)porphine. *Biochem. Biophys. Res. Commun.* **1999**, *256* (1), 84−88.
(84) Seeger, M. G.; Iglesias, B. A.; Vogel, F. S. F.; Cargnelutti, J. F. Antibiofilm action using water-soluble tetra-cationic porphyrin and antibacterial photodynamic therapy against Moraxella spp. from cattle. *Microb. Pathog.* **2023**, *178*, No. 106081.
(85) Orlandi, V. T.; Martegani, E.; Bolognese, F.; Trivellin, N.; Garzotto, F.; Caruso, E. Photoinactivation of Pseudomonas aeruginosa Biofilm by Dicationic Diaryl-Porphyrin. *Int. J. Mol. Sci.* **2021**, *22* (13), No. 6808.

https://doi.org/10.1021/acsomega.4c09535
ACS Omega 2025, 10, 22482−22507

(86) Alves, E.; Faustino, M. A. F.; Neves, M. G. P. M. S.; Cunha, Â.; Nadais, H.; Almeida, A. Potential applications of porphyrins in photodynamic inactivation beyond the medical scope. *J. Photochem. Photobiol., C* **2015**, *22*, 34−57.
(87) Donnelly, R. F.; McCarron, P. A.; Cassidy, C. M.; Elborn, J. S.; Tunney, M. M. Delivery of photosensitisers and light through mucus: Investigations into the potential use of photodynamic therapy for treatment of Pseudomonas aeruginosa cystic fibrosis pulmonary infection. *J. Controlled Release* **2007**, *117* (2), 217−226.
(88) Anas, A.; Sobhanan, J.; Sulfiya, K. M.; Jasmin, C.; Sreelakshmi, P. K.; Biju, V. Advances in photodynamic antimicrobial chemotherapy. *J. Photochem. Photobiol., C* **2021**, *49*, No. 100452.
(89) Liu, Y.; Qin, R.; Zaat, S. A. J.; Breukink, E.; Heger, M. Antibacterial photodynamic therapy: overview of a promising approach to fight antibiotic-resistant bacterial infections. *J. Clin. Transl. Res.* **2015**, *1* (3), 140−167.
(90) Fu, X. J.; Fang, Y.; Yao, M. Antimicrobial photodynamic therapy for methicillin-resistant Staphylococcus aureus infection. *Biomed. Res. Int.* **2013**, *2013*, No. 159157.
(91) Karygianni, L.; Ruf, S.; Follo, M.; Hellwig, E.; Bucher, M.; Anderson, A. C.; Vach, K.; Al-Ahmad, A. Novel Broad-Spectrum Antimicrobial Photoinactivation of In Situ Oral Biofilms by Visible Light plus Water-Filtered Infrared A. *Appl. Environ. Microbiol.* **2014**, *80* (23), 7324−7336.
(92) Dharmaratne, P.; Sapugahawatte, D. N.; Wang, B.; Chan, C. L.; Lau, K.-M.; Lau, C. B. S.; Fung, K. P.; Ng, D. K. P.; Ip, M. Contemporary approaches and future perspectives of antibacterial photodynamic therapy (aPDT) against methicillin-resistant Staphylococcus aureus (MRSA): A systematic review. *Eur. J. Med. Chem.* **2020**, *200*, No. 112341.

https://doi.org/10.1021/acsomega.4c09535
ACS Omega 2025, 10, 22482−22507